UNIVERSITÀ DEGLI STUDI DI TRIESTE

XXXVI CICLO DEL DOTTORATO DI RICERCA IN

BIOMEDICINA MOLECOLARE

TITIN DOWNREGULATION AFFECTS CARDIOMYOCYTES PROLIFERATION

Settore scientifico-disciplinare: BIO/11 BIOLOGIA MOLECOLARE

PhD student:

Alessia PALDINO, MD

Coordinatore:

PROF. Germana MERONI, PhD

Supervisore:

PROF. Gianfranco SINAGRA, MD

Co-supervisore:

PROF. Mauro GIACCA, MD, PhD

Matteo DAL FERRO, MD

Francesca Bortolotti, PhD

ACADEMIC YEAR 2023-2024

TABLE OF CONTENTS

Synopsis

In mammals, cardiomyocytes (CMs) exhibit a rapid loss of proliferation capacity following birth (1). Embryonic and fetal CMs, akin to fish and urodeles, retain a high replicative activity (2), but adult CMs are generally considered terminally differentiated cells with little to no proliferative potential(3). However, important research showed that proliferation can be re-induced in adulthood by selected miRNAs through a cumulative effect on multiple mRNA targets (4). An examination of the genes downregulated during proliferative events has revealed a massive enrichment in proteins related to skeletal and muscular function and to the assembly of the sarcomere, including, among the others, titin (TTN). Titin, the largest protein in the human body, is known as the key molecular spring in muscle cells, scaffold protein aiding myofibrillar assembly and coordinator of diverse signalling pathways. Nevertheless, despite a growing body of evidence implicating sarcomere disassembly in CM regeneration, the mechanisms governing this process and the direct link between downregulation of sarcomeric genes and re-entry into the cell cycle in adult CMs remain to be conclusively demonstrated.

In humans, truncating mutations in TTN are recognized as the most prevalent genetic cause of Dilated Cardiomyopathy (DCM), a cardiac condition characterized by left ventricle (LV) systolic dysfunction and dilation, causing a high risk of heart transplantation. These mutations mostly act through a mechanism of haploinsufficiency (5).

To date, rates of CM proliferation in DCM caused by TTN truncating variant (TTNtv) have never been addressed.

The objective of this project is to investigate whether TTN modulation mediated by specific shRNA/siRNA impacts CM proliferation and its subsequent effects on the cardiac disease phenotype. During the course of this Ph.D. project, we assessed CM proliferation induced by TTN downregulation using various models (both in vitro and in vivo) and employed multiple analytical tools to explore potential underlying mechanisms.

Initially, we generated Adeno Associated viral vector (AAV) with serotype 9 expressing shRNA against TTN for in vivo and used the siRNA for TTN in vitro for transduction of myocyte respectively. We confirmed the effective downregulation of total TTN, of both its two main isoforms present in the cardiac muscle, by RT-PCR or by immunofluorescence. Our staining clearly showed disassembled sarcomeric structures and abnormal cell morphology upon treatment.

Considering the well-established differences in CM proliferative capacity at various ages, we evaluated the impact of the selected AAV-shRNA-TTN in both neonatal and adult mice hearts (CD1 mice). In vivo, the injection of AAV9-shRNA-TTN led to an increased mortality rate in neonatal mice (up to 45%) and to the development of a DCM phenotype in the surviving animals, characterized by echocardiographic evidence of significant LV dilation and dysfunction. This was accompanied by no variation or slightly reduction in rates of CM proliferation, as assessed by EdU incorporation, without a corresponding increase in apoptosis. This resulted in compensatory hypertrophy of the remaining cardiomyocytes.

In contrast, TTN downregulation in adult mice led to an opposing phenotype characterized by hyperplastic cardiomyopathy. This unexpected phenotype was evidenced by a significant increase in LV wall thickness and near-complete obliteration of the LV cavity, driven by an elevated rate of CM proliferation, as confirmed by increased EdU incorporation, whereas no cell hypertrophy was documented. To corroborate these findings in adult mice, we took advantage of Cycle track, a fluorescent genetic reporter model developed in the Molecular Medicine laboratory (manuscript under preparation), based on the genetic labelling of cycling myocytes, to monitor cardiac proliferation. Z/EG mice carrying an inhibited lox flaked GFP were treated with AAV9-shRNA-TTN and with an AAV9 expressing a Cyclin B driven-Cre recombinase that will label permanently transduced cells by exciding a lox flanked region allowing GFP expression in proliferating CMs. Quantification of GFP-positive CMs confirmed an enhanced CM proliferation capacity in adult life following TTN downregulation.

We, then, confirmed these results testing the effect of the correspondent siRNA targeting TTN mRNA of our selected shRNA. A significant boost of CMs proliferation was clearly detected also in vitro model, particularly evident in the presence of higher grade of sarcomeric disarray.

Moreover, to deeply investigate the role of TTN downregulation in vivo at different stage of animal growth, we performed a transcriptome analysis upon shRNA-TTN administration. Analysis of neonatal hearts treated with shRNA-TTN revealed a transcriptomic profile indicative of immaturity compared to mice treated with a non-targeting shRNA, characterized by an upregulation of embryonic genes such as NANOG and SOX4. These results suggest that early TTN downregulation delays the differentiation process of CMs, maintaining a high expression level of embryonic genes until four days of life. This delay may impede the ability of CMs to form mature sarcomeric structures necessary to accommodate the physiological increase in cardiac load soon after birth, leading to LV dilation and dysfunction, causing DCM development. Conversely, adult mice treated with shTTN displayed an upregulation of pro-proliferative pathways. In particular, we reported a significant activation of

Hippo-Yap-related genes suggesting their connection with TTN and a possible key pathway governing cardiomyocyte proliferation and cardiac development involving this sarcomeric protein.

In summary, our findings underscore a differential role of TTN at various life stages, unveiling a novel mechanism of regulation of cardiomyocyte proliferation during adulthood. While its presence appears crucial for cardiac structure maturation in neonates, TTN contributes to sarcomeric stiffness in adults, likely participating in the inhibition of CM proliferation.

This research provides crucial insights into the intricate interplay between TTN and CM proliferation, shedding light on potential therapeutic avenues for cardiac diseases associated with impaired CM proliferation and sarcomere dysfunction.

Introduction

1. Cardiomyocyte proliferation

Compared to mammals, in which cardiomyocytes (CMs) loose proliferation capacity rapidly after birth (1,6,7), lower vertebrate species exhibit a persistent regenerative capabilities in their hearts. Firstly in ventricles of newt, frogs, axolotl(8–10) and after all in the zebrafish (2), cardiac regeneration has been demonstrated after a myocardial injury during their entire life (2,11,12). In particular in zebrafish model, the first experiment conducted by Poss and colleagues showed a fully progressive replacement by viable muscle tissue a apical resection of 20% of the ventricle, within 2 months and without any collagen scar. As demonstrated after (11,12), the regenerated tissue derived from the surrender differentiated CMs, and the proliferating CMs detected in it were characterized by a disassembled sarcomere and a partial detachment from the rest of the tissue. These cells showed indeed a dedifferentiated profile mainly sustained by the induction of one of the principal embryonic cardiogenic transcription factors, GATA4, maintaining a diploid mononuclear profile (13). However, if this kind of species with a unique physiological cardiac system are capable of a hyperplastic responses to injury, mammalian CMs were generally considered terminally differentiated cell with no, or only trivial, proliferative capacity(3). In the last years, this assumption has been turned around, such as the previous idea for what mammals are born with a definite number of cardiomyocytes that last for the entire life.

The first piece of this story was generated by Porello et colleagues(14,15). The scientists, performing a surgical resection of the ventricular apex or a permanent ligation of the left anterior descending coronary artery (LAD ligation) of mice postnatal day 1 (P1), showed a similar attitude of these tissues to zebrafish adult hearts. Indeed, these areas were able to face a complete regeneration countering an extensive proliferation of pre-existing cardiomyocytes, with a burst in cell cycle activity and sarcomere disassembly that is not restricted to the peri-injured zone, and obtaining a full functional recovery within 21 days, with a minimal residual scare. Notably, for both settings, regeneration response was not maintained when the experiments were performed 7 or 14 days after birth a timepoint when rodent cardiomyocytes withdraw from cell cycle (16,17).

These data were than unveiled also in other larger mammals more recently. Indeed, if the heart of P1 and P2 neonatal pigs subjected to LAD ligation showed some regenerative capacity of mice of the same age (18), more clinical interesting derived from a case report of a newborn infant (19). Just after birth, this child, manifesting severe cyanosis and oxygen desaturation, was examined immediately and diagnosed with an important anteroseptal transmural myocardial infarction (MI)

confirmed by multiple assays, such as angiography, ECG, echocardiography, and increased cardiac serum biomarkers, causing a severe compromise of heart systolic function. Amazingly, despite late thrombolytic reperfusion therapy, the heart of the newborn showed a rapidly recovering with a complete normalization at 1year of life. This case is of high interest because is of clinical knowledge that an equal clinical presentation with a LAD occlusion for more than 24 hours in an adult human will have a more dramatic and irreversible consequences, not result in functional cardiac recovery.

Therefore, these reports suggest endogenous proliferation capacity limited in short window just after birth, while adult mammal hearts exhibit a very restricted ability to regenerate themselves (4). Archeo-biological studies, by carbon dating of CM DNA (20), estimate a CM renewal capacity of 1% per year during young adulthood in humans and of 0.45% per year after 25 years of age (so that less than 50% CMs are renewed in a 70-year lifetime), and a similar rate was estimated in mice, where imaging mass spectrometry studies revealed a proliferation rate slightly under 1% every year (21).

A series of mechanisms through which it occurs and why cardiomyocytes stop undergoing an effective regenerative response in adulthood, have been investigated and discovered in the last decades. These findings if from a physiological point of view want to explain the underline causative steps, from a clinical point of view could be crucial for the development of therapeutic interventions aimed at prolonging or reawakening this regenerative window.

One crucial change occurs in the structure of cardiomyocytes. During physiological growth, in the absence of significant cytokinesis, CMs undergo polyploidization with or without nuclear division. Few days after birth in fact there is a remarkable increase of bi-nucleated cells, especially in mouse hearts (22,23), and of cells with polyploid nuclei (4n or more), in ventricular CMs in humans and primates (24). Initially, nearly all cardiomyocytes are mononucleated and diploid in rodents at birth (23), but by the second week of life, more than 90% of them become binucleated(16,25). This transformation is attributed to an increase in cell cycle activity during the first days of life. Binucleation results when a cell completes mitosis without dividing the cytoplasm, and this process is inversely related to cell cycle activity. In humans, only 25% is the extension of multinucleation and it is established during the first year of life (26). Most human cardiomyocytes undergo a final round of DNA replication without nuclear or cellular division, resulting in mononucleated cells with tetraploid DNA content. Studies have demonstrated that polyploidization in humans takes approximately 20 years (27). These structural changes not only contribute to the reduction in

cardiac regeneration but also serve as strategies to increase cell size and organ mass without compromising cellular and tissue structure, thus preserving contraction function.

Another mechanism involves the loss of centrosome integrity. Research by Engel and colleagues has linked cardiomyocyte cell cycle arrest to the disruption of centrosome integrity that occurs soon after birth (28). Key pericentriolar matrix (PCM1) proteins redistribute from the centrosome to the nuclear envelope, leading to a loss of centriole cohesion and impairing the centrosome's function as the microtubule organizing center. This, in turn, prevents further cell division. Disruption of centrosome integrity promotes cell cycle arrest through a p38-mediated G1/S checkpoint(29). In postnatal cardiomyocytes, the centriole satellite protein PCM1 is also mislocalized to the nuclear membrane, leading to a loss of the primary cilium (30), and the ability to properly assemble the contractile actomyosin ring (31). Interestingly, recent research has challenged the notion that binucleated adult cardiomyocytes are incapable of cytokinesis when properly stimulated, suggesting a more intricate scenario(32).

Changes in oxygen levels and metabolic adaptation also influence the reduction in cardiac regeneration. The transition from relatively low oxygen tension during development to higher oxygen levels after birth is accompanied by a shift from lactate anaerobic glycolysis to fatty acid oxidative phosphorylation (33). This metabolic adaptation, which enhances ATP production, leads to increased mitochondrial biogenesis and the accumulation of reactive oxygen species (ROS), resulting in oxidative stress (34). The correlation between oxygen-dependent energy production and reduced cardiomyocyte proliferation has led to the hypothesis that oxidative metabolism is linked to the loss of cardiac regeneration. Increase in ROS production seem to result in oxidative DNA damage and cell-cycle arrest (35). This damage can be delayed by ROS scavenging or the inhibition of DNA damage response pathways. Additionally, exposure to hypoxia can reduce mitochondrial metabolism and oxidative DNA damage, potentially promoting cardiac regeneration (36). These findings collectively suggest that withdrawing cardiomyocytes from the cell cycle may be an adaptive response to prevent DNA damage in mature aerobic cells.

The extracellular matrix (ECM) also plays a role in regulating cardiomyocyte cell cycle and regeneration. The ECM defines the mechanical properties that cardiomyocytes endure and regulates the effect of growth factors. Culturing cardiomyocytes on matrices of varying stiffness influences dedifferentiation, myofibrillar disassembly, and cell division (37). Changes in ECM composition and stiffness, with a marked deposition of collagen, between postnatal days 1 and 2 in mice have been shown to affect regenerative capability (38). The ECM's role in regulating cardiomyocyte cell cycle and regeneration is an area of ongoing investigation.

Furthermore, the immune system has a significant impact on cardiac regeneration. Macrophages, in particular, play a critical role in the regenerative process in zebrafish and neonatal mouse hearts. Neonatal mice possess embryonic-derived macrophages in the heart, which are essential for efficient cardiac repair with low inflammation level. Even the adult heart maintains embryonic resident macrophages with similar properties. However, after injury, the massive recruitment of monocytes and monocyte-derived macrophages takes over, leading to a robust inflammatory response that impairs cardiomyocyte renewal and angiogenesis (39). The precise role of inflammatory cells in cardiac healing is not fully understood, but understanding the differences between regeneration-permissive and regeneration-restrictive immune environments is crucial and may offer insights for potential interventions to stimulate cardiac repair in adults.

These nuclear, metabolic, matrix and immune system changes, together with the highly complex and stable cytoarchitecture of mature CMs, seem to be the main reasons behind the cessation of proliferative potential (3). Indeed, CMs' maturation is characterized also by an increase of size, number and complexity of myofibrils, which in turn rely on a gradual growth of cytoskeletal, sarcomeric and intercalated disk's structures (40). This terminally differentiated phenotype, for several years, has been associated with an irreversible state in terms of replicative activity (3).

The shift from neonatal to adult life places significant demands on the heart, necessitating rapid adjustments to cope with increased circulatory requirements, heightened blood pressure, and augmented ventricular wall stress. To meet these challenges, the postnatal heart undergoes substantial structural reconfiguration of its cytoskeleton and sarcomeres, entailing an expansion in the number of fibers and contractile units, as well as a transition in the expression of specific sarcomeric protein isoforms from fetal to adult versions. These changes are accompanied by modulation of CMs size passing from a small dimension to a rod-shape typical of the adult age, with aligned sarcomeres, transverse tubules and intercalated discs that allowed CMs connection for a simultaneous contraction (Figure i).

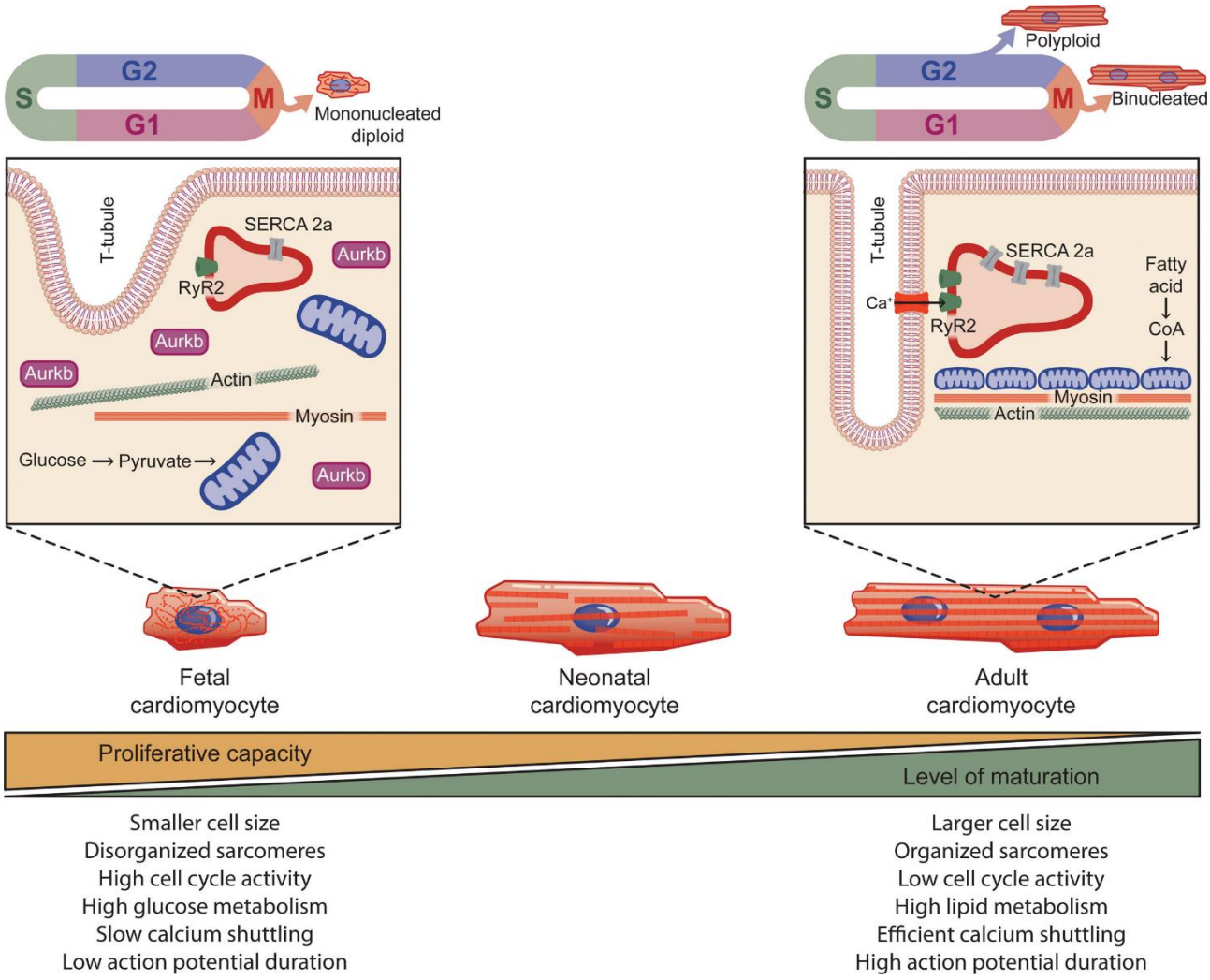

Figure i. Proliferation-maturation dichotomy in cardiomyocytes. (adapted from Singh et all, 2023)

An exemplary instance of this isoform transition in the sarcomere can be observed in the heavy chain of myosin (MHC), a critical constituent of thick filaments within sarcomeres. In rodents, shortly after birth, there is a predominant shift from the β-MHC isoform (MYH7), known for its slower-twitch properties, to the faster α-MHC isoform (MYH6). This shift establishes an isoform ratio of 1:9 (41). In contrast, the human ventricular myocardium predominantly maintains the β-MHC isoform, accounting for approximately 95% of the MHC composition (42). This variation can be attributed to the significantly higher heart rate in rodents compared to humans. However, it is also vital for sustaining optimal cardiac function.

Furthermore, the Troponin complex, a calcium-sensitive regulator of contraction, encounters an isoform transition during mammalian development, shifting from the slow skeletal isoform (ssTnI) to the cardiac muscle isoform (cTnI) encoding by TNNI1, TNNI2 and TNNI3 (43). With

development, the ratio of ssTNI to cTNI decreases with no detectable levels of ssTNI in the adult heart (44). These changes ultimately contribute to changes in cell shape, increased stroke volume, and cardiac output during embryonic and early postnatal development (45).

Titin, an extensive sarcomeric protein spanning from the Z-line to the M-line (see paragraph below), plays a pivotal role in regulating passive ventricular tension and cardiac compliance. In the fetal heart, the primary isoform of titin is N2BA, known for its larger size and greater compliance, whereas the adult heart predominantly expresses the N2B isoform, associated with higher passive tension (46).

Significantly, the disassembly of sarcomeres is a prerequisite for the formation of the mitotic spindle and contractile ring during cardiomyocyte division. Nevertheless, the exact mechanisms governing the structural dismantling of sarcomeres and their subsequent reassembly during cardiomyocyte proliferation remain largely elusive. This adaptive shift in adult cardiomyocytes, driven by heightened workload, may present a physical barrier to dedifferentiation and re-entry into the cell cycle. In support of this concept, the Sadek group conducted an analysis of human tissue samples from patients with heart failure who had left ventricular assist devices as a model of unloading and consistently observed the stimulation of cardiomyocyte proliferation (47).

The heart's capacity to adapt its sarcomeric structure and protein isoforms in response to evolving demands underscores the remarkable resilience of cardiac physiology and adaptation, with profound implications for our comprehension of cardiac development and regeneration.

Finally, the cytoskeleton, a complex network of structural proteins within the cell, also plays a pivotal role in this essential process.
During the interphase, nonsarcomeric actin forms an extensive network in cardiomyocytes, which rapidly disassembles as they enter mitosis and assume a rounded shape. This phenomenon is a common feature in many cell types, where there is a reciprocal relationship between the cell cycle machinery and the actin cytoskeleton. The state of organization of the cytoskeleton plays a crucial role in regulating cell cycle progression. Disruptions in proper cytoskeleton reorganization can result in cell cycle arrest by activating checkpoints in both the G1 and G2/M phases of the cell cycle. For example, overexpression of Cofilin 1, an actin-depolymerizing factor (ADF), leads to cell cycle arrest in the G1 phase, while increased F-actin polymerization, whether due to genetic mutations or treatment with substances like Jasplakinolide, causes delayed mitosis and defective cytokinesis, ultimately leading to cell multinucleation (48).
This connection between altered nonsarcomeric actin dynamics and cell division defects holds significant implications for CMs. It could potentially explain why CMs exhibit nuclear division in

the absence of cytokinesis and experience a block in the G2 phase when they halt their proliferation. Notably, over 150 proteins contain an actin-binding domain that influences nonsarcomeric actin dynamics and mediates signaling (49). The dynamic formation of the actin cytoskeleton and its rapid responsiveness to cellular cues, particularly those related to extracellular environment sensing, depend on the ratio between polymerized filamentous actin (F-actin) and monomeric globular actin (G-actin). This ratio also plays a role in regulating CM proliferation. Recent research has demonstrated that several microRNAs can stimulate CM proliferation when overexpressed in neonatal rat and mouse CMs (4). These microRNAs typically share the characteristic of downregulating factors that inhibit actin polymerization by directly interacting with G-actin, including Cofilins, Twinfilins, Thymosin β4, and Profilins. Furthermore, these pro-proliferative microRNAs downregulate proteins such as cysteine and glycine-rich protein 3, MT-associated monooxygenase, calponin, LIM domain-containing 3, and Aurora A kinase, which are directly or indirectly involved in the regulation of actin polymerization (50). One of the direct targets of four highly effective microRNAs (miR-199a-3p, miR-1825, miR-302d, and miR-373) that stimulate CM proliferation is Cofilin2. Cofilin2 is a muscle-specific member of the ADF/Cofilin family of proteins responsible for modulating actin filament equilibrium by preventing the assembly of actin monomers and promoting the depolymerization of actin filaments. Downregulation of Cofilin2 through RNA interference significantly enhances actin polymerization, resulting in the formation of cortical stress fibres and the disorganization of the sarcomeric architecture. This disruption is sufficient to induce neonatal CMs to enter the cell cycle (50).

The exact mechanism by which actin polymerization leads to CM proliferation remains an active area of research. Interestingly, it is suggested that the myocardin-related transcription factors (MRTF-A and MRTF-B) are critical in connecting actin polymerization with the activation of proliferation. Typically, these transcription factors are sequestered in the cytoplasm through their specific interactions with G-actin monomers. However, when actin polymerizes, which often occurs in response to increased substrate stiffness via the RhoA and ROCK pathway (51), these factors are released from G-actin binding and translocate into the nucleus. Inside the nucleus, they act as co-activators of the serum response factor (SRF). SRF controls the expression of genes that contain CArG boxes in their promoters, influencing myogenic specification, cytoskeletal organization, and cell proliferation. This suggests that, in CMs, MRTF may link actin polymerization with proliferation, although more research is needed to elucidate the exact mechanisms involved.

Another crucial molecular component that connects the sensing of mechanical cues, actin cytoskeleton dynamics, and cell proliferation is the Hippo pathway. This pathway serves as a key

regulator of CM proliferation during heart development. In CMs, the positive effectors of the Hippo pathway are YAP (yes-associated protein) and TAZ (transcriptional co-activator with PDZ-binding motif). In their dephosphorylated form, YAP and TAZ translocate to the nucleus, where they associate with the TEAD1–4 transcription factors, driving the transcription of genes involved in cell proliferation (52). Knockout of cardiac-specific YAP leads to myocardial hypoplasia and contractile dysfunction in embryonic mice, while YAP overexpression induces heart regeneration in neonatal and adult hearts (53).

Also, PI3-Kinase-Akt pathway is pivotal for cell growth and survival. Akt, a key component of this pathway, inactivates proapoptotic proteins, activates CDK2, inhibits p27, and regulates cell growth through mTOR activity. Akt also plays a role in stabilizing β-catenin via GSK-3β inactivation and in activating Cyclin D1. PI3K, downstream of various receptor tyrosine kinases, including ErbB2 and ErbB4, crucial for cardiac development and cardiomyocyte proliferation. Epidermal growth factor receptors ErbB2 and ErbB4, found on cardiomyocytes, interact with Neuregulin-1 (NRG1) to support cardiomyocyte proliferation during embryogenesis. While NRG1-induced proliferation diminishes after birth due to reduced ErbB2 expression, external activation of NRG-1/ErbB2-4 signaling induces quiescent cardiomyocytes to reenter the cell cycle via PI3K-Akt, leading to cardiac regeneration (54). Additionally, Yap increases IGF receptor abundance, that utilizes the PI3K-Akt pathway to inactivate GSK-3β, stabilizing β-catenin, reinforcing positive regulation of cardiomyocyte proliferation vital for chamber morphogenesis (53). Cardiac overexpression of IGF-1 in mice stimulates proliferation, prevents cell death, and mitigates ventricular dilation after infarction (53).

In conclusion, the orchestration of a complete replicative cycle in CMs hinges upon the intricate remodeling of their cytoskeleton and sarcomere, a process significantly aided by the transient disassembly of myofibrils (55). While this phenomenon has traditionally been attributed to embryonic, fetal, and early neonatal mammalian CMs, nature's diversity reveals fascinating exceptions, notably in the hearts of certain fish and newts. In these unique species, the remarkable phenomenon of cardiac regeneration endures into adulthood, fueled by the downregulation of specific cytoskeletal and sarcomeric genes (56,57). Although significant strides have been made in the study of cytoskeletal protein modulation and the intricate mechanisms linking the cell cycle with cytoskeletal dynamics, the enigma of how sarcomere disassembly, along with the concurrent reduction in the transcriptional activity of sarcomeric genes and a decline in myofibril density, can stimulate CM proliferation in adult life remains largely unresolved. This captivating conundrum continues to beckon researchers to explore the intricate connections between these processes and uncover the secrets of cardiac regeneration.

2. TTN and Dilated Cardiomyopathy

Titin (TTN), acknowledged as the largest sarcomeric protein and a pivotal constituent of myocardial tissue, plays a crucial role in cardiomyocytes. Spanning approximately half of the sarcomere, TTN is positioned between the Z-disc and M-band, conferring passive elasticity to myofibrils and facilitating multiple mechanosensory signaling pathways (21). TTN is encoded by a single gene, located on the long arm of chromosome 2 and comprising 364 exons (22). Notably, alternative splicing of this gene, especially concerning exons located within the I-band region, gives rise to two predominant TTN isoforms: the more extensive and compliant N2BA isoform and the shorter, stiffer N2B isoform (23). The distribution, quantity, and relative proportions of these isoforms during perinatal development and adulthood have been thoroughly investigated by Opitz C. A. et al. in rat hearts (24). In perinatal rat hearts, the N2BA isoform predominates, reflecting the immediate post-birth physiological demands, including elevated filling pressures and reduced extracardiac constraints (25). To counteract the risk of heart overextension, a swift upregulation of the N2B isoform occurs (26,27).

Both N2BA and N2B isoforms encompass four distinct regions (Figure ii):

- Z-disk: The amino-terminus of TTN is incorporated within the sarcomeric Z-disk, playing a pivotal role in myofibril assembly, stabilization, and maintenance (58);
- I-band: An elastic component functioning as a bidirectional spring, restoring sarcomeres to their resting length after systole and limiting their stretch in early diastole (59);
- A-band: An inextensible segment that binds myosin and myosin-binding protein, critically important for biomechanical sensing and signaling (60);
- M-band: This region of the protein houses a kinase essential for strain-sensitive signaling, gene expression, and cardiac remodeling in dilated cardiomyopathy (DCM) (61–63).

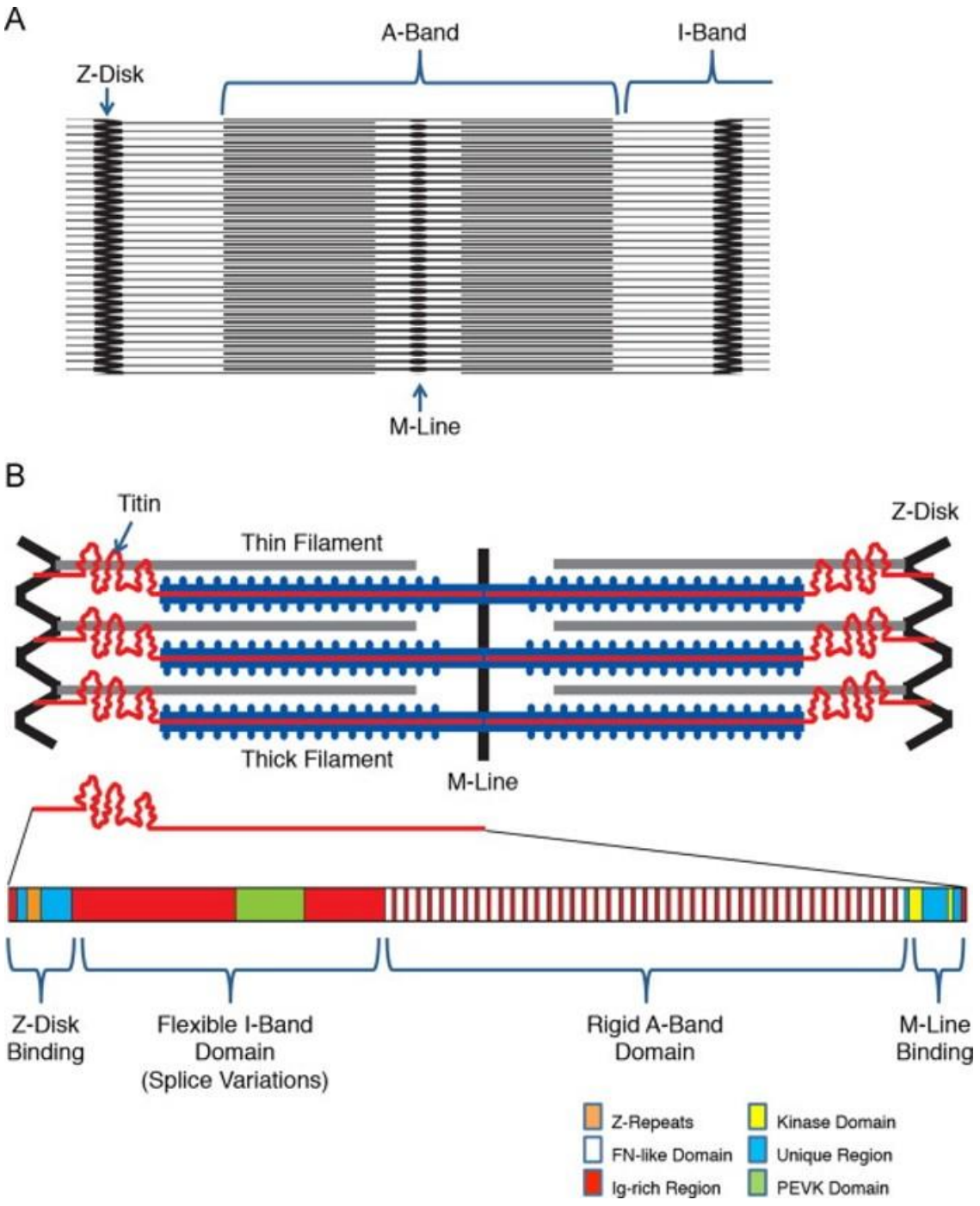

Figure ii: Titin regions. (adapted from Myhre 2014)

DCM is a heart muscle disease characterized by left ventricular (LV) dilatation and progressive systolic dysfunction in the absence of abnormal loading conditions, such as hypertension and valve disease, or coronary artery disease sufficient to cause global systolic impairment (64). Genetic forms of DCM can be divided in (65):

- Familial DCM: that is diagnosed when two or more family members are affected;

- Sporadic DCM: when a unique family member is affected, although it may represent the manifestation of a de novo mutation.

Almost 50 genes, most of which encode components of sarcomere, cytoskeleton or nuclear lamina, have been shown to be disease related (66). Most of these mutations are transmitted as dominant trait, a few show recessive, X-linked or mitochondrial transmission (matrilineal inheritance). Starting from 2012, it has been finally showed the important role of TTN as major cardiac disease gene (5). Mutations in TTN are now recognized as the most common genetic cause of DCM, accounting for approximately 15% of DCM cases in one of the largest series of unselected patients (67,68). The pathogenicity of these mutations is primarily associated with truncating variants (TTNtv) that, if transcribed and translated, produce truncated proteins. These variants include nonsense mutations, frameshift insertions and deletions, and canonical splice-disrupting variants (69). Intriguingly, TTNtv have also been detected in about 1% of the general population without apparent cardiomyopathy (60,69). This has prompted the need to distinguish between disease-related and benign TTN variants. It might seem that clinical significance of TTNtv is largely predicted by exon usage and variant location, in term of distance of the TTNtv from the protein N-terminus.

It appears that the clinical relevance of TTNtv is largely influenced by exon usage and the variant's location, particularly in terms of its proximity to the protein's N-terminus. Previous research indicated that severe and familial DCM is primarily associated with TTNtv located in the A-band (5). TTNtv affecting both N2BA and N2B isoforms are more prevalent in DCM patients and exhibit a stronger association with the condition than TTNtv affecting only the N2BA isoform (60). To aid clinicians in understanding the molecular and clinical implications of specific TTNtv, each exon is characterized by a 'proportion spliced in' (PSI) score (60). The PSI score represents the mean incorporation of each TTN exon, denoting the proportion of transcripts that include each exon (60). This data is derived from transcriptomic analysis of LV tissue from DCM patients. A PSI > 15% has been established as the minimum threshold for pathogenicity, while a PSI > 90% describes exons with high cardiac expression and a stronger association with fully penetrant DCM phenotypes (70). The entire A-band, as well as the proximal or terminal part of the I-band, contain exons with PSI values approaching 100%, while TTNtv in M-band exons and Z-band exons necessitate a case-by-case evaluation (70).

Hence, the hallmark features of TTNtv-induced DCM are incomplete penetrance and variable disease manifestations, with mild phenotypes being the most common (71). TTNtv are comparatively rare in pediatric DCM, becoming almost completely penetrant after the age of 70 (Cannata') (72,73) (5,60,71). However, it is noteworthy that in a small proportion of cases, certain

TTNtv may be linked to an arrhythmogenic phenotype of DCM, particularly in the presence of additional environmental factors (68,74). Such DCM forms associated with TTNtv also exhibit lower ventricular mass and wall thickness, along with increased interstitial fibrosis. The mechanisms underlying this attenuated hypertrophic response to increased wall stress remain incompletely understood (68,74).

Consequently, current international guidelines recommend continuous clinical monitoring of patients with TTNtv-related DCM and their family members, even in the absence of overt cardiomyopathy (74). In contrast, TTN missense variants are presently considered mostly benign (70).

From a molecular perspective, the pathogenic mechanisms linking the presence of TTNtv to DCM development remain the subject of ongoing debate. Two main hypotheses have been proposed:

-Reduced total TTN protein dose: Mutated alleles with TTNtv may undergo nonsense-mediated decay, preventing the expression of abnormal proteins.

-Normal total TTN protein dose: Abnormal proteins may be produced, but they could be inactive due to a 'loss of function.' Alternatively, they may exert deleterious effects through a 'poison-peptide' or 'dominant negative' mechanism, such as forming aggregates or inhibiting the function of wild-type proteins.

However, current literature predominantly supports the notion that TTN haploinsufficiency underlies the pathogenic mechanism of TTNtv-related DCM (75). Some TTNtv variants seem to result in the production of stable truncated proteins that cannot effectively integrate into well-organized functional sarcomeres (75). This inadequacy in sarcomere assembly contributes significantly to the profound contractile deficit observed in affected cardiomyocytes, thus contributing to the development of DCM.

AIM OF THE THESIS

A recent investigation, focused on the potential of specific miRNAs to augment CM proliferation, has unveiled that this phenomenon arises from the cumulative impact on multiple mRNA targets within the cells (4). This comprehensive analysis of genes downregulated by these miRNAs has demonstrated a noteworthy enrichment in genes associated with categories such as 'skeletal and muscular system development and function' and 'cellular assembly and organization.' Among these genes is TTN, a pivotal player. Notably, targeted downregulation of these genes has the potential to independently induce CM proliferation.

In humans, it is well-established that TTNtv represent a preeminent genetic ethology of DCM, with their pathogenicity primarily attributed to haploinsufficiency mechanisms(75). The aim of this study is to probe the repercussions of reducing TTN levels, particularly with regard to cardiac myocyte turnover and proliferative dynamics, and if these replicative abnormalities could be a causative association with TTNtv-DCM.

To induce a targeted reduction in TTN expression, we have employed a precise strategy involving the administration of TTN-specific siRNA/shRNA respectively in vitro and in vivo models. This approach enabled us to comprehensively evaluate cardiac phenotypic alterations, conduct an in-depth examination of CM structural changes, and explore the proliferative capacities of the cells under regulated TTN downregulation.

Methods

1. Production and purification of AAV vectors

All AAV vectors were produced by the AVU unit at the ICGEB, Trieste, Italy (http://www.icgeb.org/avu-core-facility.html) as described previously (G. P. Gao et al., 2002). Briefly, infectious AAV6 and AAV9 vector particles were generated in HEK-293 cells by co-transfecting each vector plasmid together with the packaging plasmids expressing AAV and adenovirus helper functions, pDP6 (PlasmidFactory). Viral stocks were obtained by CsCl2 gradient centrifugation; AAV titers, determined by measuring the copy number of viral genomes in pooled, dialyzed gradient fractions were in the range of 1x1012 to 1x1013 genome copies per millilitre.

Cardiomyocytes were transduced with AAV6-control (empty vector), AAV6-GFP and AAV6-sh Luc and sh TTN. the day after plating using a multiplicity of infection (MOI) of 5x 104 viral genomes particles per cell. The day after transduction the medium was changed. The correspondent AAV9 were generated in parallel and used for in vivo transduction of cardiac tissue as previously established in the laboratory (3.0 x 1011 and 3.9 x 1012 viral genomes particles per animal).

2. shRNA vector construction

TTN siRNA candidates were obtained from the mouse genome-wide siRNA library stock plates (siGENOME SMARTPools, Dharmacon, Thermo Scientific) of specific gene siRNA pool.

Each siRNA from the pool was deconvoluted and tested on cardiac neonatal cells in vitro and the most efficient, in the downregulation of TTN transcription (attested at almost 20%), was selected for the followed experiments. The TTN target region of the selected siRNA was exon 341 (Ig-like 151), common for all TTN isoforms, with this sequence: GCGGAAAGTACACAATTAA. Starting from this sequence, the correspondent shRNA was designed. The sequence against Luciferase, AAATCGCTGATTTGTGTAGTC, was used as control shRNA (shLUC). The shRNA cassette was inserted at 3-prime of an AAV backbone plasmid. Double-stranded fragment with cohesive ends were then cloned into the same restriction enzyme sites of a self-complementary AAV vector under the control of the human U6 promoter, followed by a ZsGreen expression cassette that serves as a marker to monitor the shRNA delivery efficiency. For in vivo experiments the ZsGreen cassette was removed to avoid cellular toxicity.

3. siRNA transfection

Transfection of mouse siRNAs was performed using a standard reverse transfection protocol, at a final siRNA concentration of 50 nM. For experiments performed in 96-well plates, 15 µl of 500 nM siRNAs were transferred to 96 well plates. Transfection reagent, Lipofectamine RNAiMAX Transfection Reagent (0.2 µl per 96-well, Life Technologies) diluted in 35 µl of OPTI-MEM (Life Technologies) was then added to the siRNAs arrayed on 96-well plates and incubated at RT for 30 min. Mouse CMs, suspended in 100 µl antibiotic-free culture medium, were then seeded onto the 96-well plates at 25000 cells per well and incubated at 37°C, 5% CO2. Transfections performed in 6-well plate format were done using the same procedure but transferring 7 ul from the 20 µM siRNAs stock to each well. 5.7 µl of Lipofectamine RNAiMAX were diluted in 600 µl of OPTI-MEM and then added to siRNAs. 30 min. after, 600000 neonatal mouse cardiomyocytes, resuspended in 2.5 ml of culture medium, were seeded on the transfection reagents in the plate. A non-targeting control siRNA (NTC-siRNA) was used as control vector.

4. Adult cardiomyocyte isolation

We adapted the protocol "Langendorff-Free Method for isolation of viable CMs" from Ackers-Johnson et al (76). In brief, the heart was perfused with warm EDTA, perfusion buffer and a digestion buffer (including collagenase I, IV and protease 14) through LV when aorta was clamped, then heart tissue became softened and swollen. After that, heart tissue was teared into pieces and dissociated by pipetting. Cell suspension was then passed through 100 µm strainer and processed to three rounds of gravity settling. Cardiomyocytes, in the pellet, were harvested for RNA extraction.

5. Neonatal cardiomyocyte isolation

Primary cardiomyocytes were isolated from heart of neonatal mouse and rats using the Neonatal Heart Dissociation Kit (Miltenyi Biotec) according to the manufacturer's instructions. The purpose of this procedure is to dissociate the neonatal hearts into single-cell suspensions by combining enzymatic degradation with mechanical dissociation, to disrupt the extracellular matrix, which maintains the structural integrity of the tissue.

Briefly, hearts from 1-to-2-day old CD1 mice or Wistar rats were retrieved and transferred into a 10 cm dish containing PBS; ventricles were separated from both the atria and the great vessels, cut into pieces of ~2 mm diameter and collected in a fresh tube. The digestion mix, obtained by combining the enzyme mix 1 (Enzyme P + Buffer X, previously heated at 37° C for 5 minutes) and the enzyme mix 2 (Buffer Y + Enzyme A + Enzyme D), was transferred together with the harvested tissue into the MACS C Tube where the fragments dissociation was performed. The C Tube was attached onto

the sleeve of the gentleMACS™ Dissociator for the mechanical dissociation steps; afterwards the digestion was run at 37°C for 1h.

After the run termination, 7.5 ml of Dulbecco's modified Eagle medium 4.5 g/l glucose (DMEM, Life Technologies), containing 5% FBS, 20 mg/ml vitamin B12 (Sigma), 100 U/ml penicillin and 100 µg/ml streptomycin (Sigma), were added to the Tube. Then, the digested tissue was filtered through a 40 µm, cell strainer (BD Falcon) to remove any remaining larger particles from the single-cell suspension. After that, the cell strainer was washed with 3 ml of DMEM and the filtrate was centrifuged at 600 x g for 5 minutes to pellet the cells, which were then resuspended in a Red Blood Cell Lysis Solution to remove erythrocytes and incubated for maximal 2 minutes at room temperature. The next steps were to wash the cells twice by centrifugation and resuspension in an PBS solution + Enzyme A and later in complete medium. The collected cells were pre-plated on 100-mm plastic dishes at 37 °C in 5% CO2 and humidified atmosphere for 2 hours, to allow the attachment of fibroblasts. After the pre-plating step, the cardiomyocyte-containing supernatant was collected, and cells were counted. CMs cells were plated at the appropriate density in Primaria 96-well plates (BD Falcon) or Primaria 6-well plates (BD Falcon), according to the experiment.

6. Rat engineered heart tissue

Rat fibrin-based engineered heart tissue (EHT) has been produced by Molecular Cardiology group at ICGEB, Trieste, Italy. To generate fibrin-based EHTs a reconstitution mixture was prepared on ice as follow. Final concentration of cells: 4.1^106 cells/mL, 5 mg/mL bovine fibrinogen (Sigma F8630), DMEM 2X (20% DMEM 10x, 20% heat inactivated horse serum [Thermo Fisher 26050-088], 1% penicillin/streptomycin [Thermo Fisher 15140-122]). Casting molds were prepared by adding 1.5 mL 2% agarose in PBS (Invitrogen 15510-027) per well in 24-well culture dishes and placing Teflon spacers inside. After agarose jellification, the spacers were removed (LxWxD 12 x 3 x 4 mm) and silicone post racks were placed onto the dishes with pairs of posts reaching into each casting mold. For each EHT 100 µL reconstitution mix was mixed briefly with 3 µL thrombin (100 U/mL, Sigma Aldrich T7513) and pipetted into the agarose slot. For fibrinogen polymerization, the constructs were placed in a humidified cell culture incubator at 37°C, 7% CO2 for 2 hours. To ease removal of the constructs from agarose casting molds, cell culture medium (300 µL) was then added in each well. Racks were transferred to new 24-well cell culture dishes. EHTs were maintained in 37°C, 7% CO2 humidified cell culture incubator. Media was changed every two days. EHT medium consisted of DMEM (Biochrom F0415), 10% horse serum (Thermo Fisher 26050-088), 1% penicillin/streptomycin (Thermo Fisher 15140-122), insulin (10 µg/mL, Sigma-Aldrich

I9278), and aprotinin (33 µg/mL, Sigma Aldrich A1153). EHTs were visually expected every day and are considered mature approximately 10 days after the development of coherent beating.

7. Animal studies

Animal care and treatment were conducted in conformity with institutional guidelines in compliance with national and international laws and policies (EEC Council Directive 86/609, OJL 358, 12 December 1987), upon approval by the ICGEB Animal Welfare Board and Ethical Committee as well as by the Italian Minister of Health. CD1 mice were obtained from Harlan and maintained under controlled environmental conditions.

Cd1 pups were injected intra-peritoneally immediately after birth with 30ul of the indicated AAV9 vectors. Edu was injected at day 0 and day 2 and animals were sacrificed at day 3. A group of animals received the same treatments and was followed by echocardiography up to 3 months.

Adult Cd1 mice (12 weeks) received AAV9 vectors by intravenous injection (final volume of 150 uL) and received Edu every other day from week 2 up to week 5. All animals were monitored by echocardiography up to 3 months.

8. Myocardial infarction

Myocardial infarction was produced in adult CD1 (12 weeks old), by permanent left anterior descending (LAD) coronary artery ligation. Briefly, mice were anesthetized with an intraperitoneal injection of ketamine and xylazine, endotracheally intubated and placed on a rodent ventilator. Body temperature was maintained at 37°C on a heating pad. Beating heart was accessed via a left thoracotomy. After removing the pericardium, a descending branch of the LAD coronary artery was visualized with a stereomicroscope (Leica) and occluded with a nylon suture. Ligation was confirmed by the whitening of a region of the left ventricle, immediately post-ligation. Contextually to myocardial infarction, mice received intravenous injection of AAV9 vectors.

9. Z/EG model

To track proliferating cardiomyocytes in adult hearts upon shTTN administration we established an experiment in adult Z/EG carrying a lox GFP in their genome. These mice animals underwent AAV9-shTTN administration and were monitored over time for cardiac function. Once established the model, adult animals received shTTN or shRNA control simultaneously received AAV9 expressing the Cre recombinase under the control of the Cyclin B promoter to label only GFP+ proliferating CMs or with an AAV9 expressing a CMV driven-Cre recombinase to monitor and quantify the recombination capacity of the system. This system is allowing genetic labelling of

proliferating myocytes. The expression of lox flaked GFP is normally inhibited and can be activated only in the presence of Cre that will permanently allowed the GFP expression in all the transduced CMs.
At day 30 upon injection animals were sacrificed, the heart perfused with formalin and tissue were paraffin embedded. Cardiac proliferation was monitored by IF by staining for alpha actinin (CMs), DNA duplication (Edu) or by quantifying the number GFP+ labelled CMs. The CMV-Cre reporter was used as AAV transduction normalizer.

10. Histological and immunofluorescence analysis

Animal were sacrificed and the hearts were briefly washed in PBS, weighted, fixed in 10% formalin at room temperature, embedded in paraffin and further processed for histology or immunofluorescence. Mouse heart sections were deparaffinized in xylene and rehydrated and further processed for histology. Haematoxylin–eosin staining (Bioptica) was performed according to standard procedure and analysed for morphology.

For immunostaining, antigen retrieval was performed by boiling samples in sodium citrate solution (0.1 M, pH 6.0) for 20 min. Sections were let cool down and permeabilised for 20 min in 1% Triton X-100 in PBS, followed by blocking in 1% BSA (Roche). Sections were then stained overnight at 4°C with primary antibodies diluted in blocking solution, recognizing the following antigens: sarcomeric α-actinin (Abcam), lectin Wheat Germ Agglutinin (WGA- Fitc conjugated), titin. Sections were washed with PBS and incubated for 2 h with the respective secondary antibodies conjugated with Alexa Fluor-594 (Life Technologies). Nuclei were identified by counter-staining sections with Hoechst (Life Technologies) and slides were then mounted in Vectashield with DAPI (Vector Labs). Wheat Germ Agglutinin was used to measure CM cross sectional area using ImageJ.

For EdU incorporation analysis, tissue sections were deparaffinized, antigen retrieval was performed as previously described, permeabilization was performed in 1% triton for 20 minutes and then hearts were stained overnight at 4°C with anti-α-actinin antibody (Abcam) in 5% horse serum PBS. Washes and secondary antibody incubation were performed as described above. Edu staining was performed following the manufactures instructions. Hoechst was used to labelled cell nuclei.

For the quantification of immunofluorescence, we used at least 3 animals per group and at least 8 sectors for each heart section were quantified. All quantifications were performed in blind.

11. TUNEL assay for apoptosis detection

TUNEL assay was performed on pups heart sections. Tissues were fixed with 4% paraformaldehyde (PFA) and permeabilized with 0.5% Triton X-100 for 10 min. After 1 h in blocking solution (2% BSA) at room temperature, hearts were stained with the primary antibody against sarcomeric a-actinin (1:200, EA-53 Abcam) for 2 hours. Alexa Fluor-488 donkey anti-mouse (1:500, A-21202 Thermo Fisher Scientific) was used as a secondary antibody. Apoptotic cells were visualized by in situ cell death detection kit, TMR red (Roche Diagnostics), according to the manufacturer's instructions. Nuclei were stained with Hoechst 33342 (1:5000 in PBS, Life Technologies).

12. Echocardiography

To analyse LV function and dimension, transthoracic two-dimensional echocardiography was performed in mice sedated with 5% isoflurane, using the Vevo 770 Ultrasound (Visualsonics), equipped with a 30-MHz linear array transducer. M-mode tracing were used to measure LV anterior and posterior wall thickness, LV internal diameter at end-systole and end-diastole and calculate fractional shortening in short axis view. B-mode tracing and Simpson-method was used to calculate LV systolic and diastolic volumes and ejection fraction. Left atrium dilatation was used as indicator of diastolic dysfunction (77).

13. RNA isolation and quantitative real-time PCR

Total RNA, including small RNA fraction, was extracted from total hearts or purified CMs using Trizol reagent and the miRNeasy Mini Kit (Qiagen), according to the manufacturer's instructions.

Primary cardiomyocytes seeded onto 6-well were washed twice in PBS and then cells were lysed in 1 ml of TRIzol Reagent (Life Technologies) and incubated for 3 min at RT. Heart sections of CD1 mice were lysate with 1 ml TRIzol and dissociated using MagNA Lyser green beads (Roche) at 6500 rpm for 60 seconds. After this, the heart homogenate was put in 1.5 ml tubes and incubated for 3 minutes at RT. From here the procedure of RNA extraction from primary cells or heart tissue is the same, although specified. 0.2 ml of chloroform per ml of TRIzol was added to cells lysate (or heart homogenate). The tubes were shaken vigorously for 15 s and incubated for 10 min at RT. Samples were then centrifuged at 12,000 x g for 10 min at 4°C. After the centrifugation, the upper aqueous phase, was transferred to a new tube and 0.5 ml isopropanol was added. The tubes were shaken vigorously for 15 s and incubated for 10 min at RT. Samples were then centrifuged at 12,000 x g for 10 min at 4°C. After the centrifugation, the upper aqueous phase was removed, and 1 ml of 75% Ethanol was added. Samples were then centrifuged at 12,000 x g for 5 min at 4°C. After the centrifugation, the upper aqueous phase was removed, and 0.6 ml of 75% Ethanol was added. Samples

were then centrifuged at 12,000 x g for 5 min at 4°C. After the centrifugation, the upper aqueous phase was removed, and tubes were then left opened under chemical hood to allow the complete evaporation of the EtOH. Finally, 40 µl or 70 µl of RNase-free water were added to resuspend the RNA obtained from primary neonatal cardiomyocytes or from heart tissue, respectively.

For quantification of gene expression in isolated CMs, total RNA was reverse transcribed using hexameric random primers followed by qRT–PCR using predesigned TaqMan assays (Applied Biosystems) for titin or genes related to apoptosis (Bax, Bcl), according to the manufacturer's instructions. The housekeeping gene Gapdh was used for normalization.

14. Transcriptomic analysis

Firstly, RNA was extracted (as mentioned above) from CMs of these 7 groups of 4 mice each:

- Neonatal mice at p4 treated at p0 with an intra-peritoneal injection of AAV9-shTTN;
- Neonatal mice at p4 treated at p0 with an intra-peritoneal injection of AAV9-shLUC;
- Neonatal mice at p4 treated at p0 with an intra-peritoneal injection of AAV9-shTTN;
- Neonatal mice at p4 treated at p0 with an intra-peritoneal injection of AAV9-shLUC;
- Adult mice, 10 weeks old, 14 days after intra-venous injection of AAV9-shTTN;
- Adult mice, 10 weeks old, 35 days after intra-venous injection of AAV9-shTTN;
- Adult mice, 10 weeks old, after 14 days from intra-venous injection of AAV9-shLUC;

RNA concentrations were quantified by Nanodrop NanoDropTM ND-1000 (Thermo Fisher Scientific, Waltham, MA, USA), and quality was assessed using Agilent 4200 TapeStation system. Libraries were generated using Illumina Stranded mRNA Prep and were sequenced on a Novaseq 6000 sequencer (Illumina, Inc., San Diego, CA, USA), producing 2x150 bp paired-end reads. De-multiplexing and production of FASTQ sequence files, establishing raw sequencing quality and alignment to the human reference genome hg38 were performed using Illumina BCL2FASTQ v2.20, FastQC (version 0.11.9)/MultiQC (version 1.0.dev0) and Rsubread (v.2.10.5) package, respectively. Gene counts were extracted using the feature counts function based on Gene annotations.

15. Statistical analysis

Data are presented as mean ± standard error of the mean (SEM). Statistical analysis was performed by employing commercially available software (GraphPad Prism). Data were first checked for normal distribution, then differences among groups were compared by one- and two-way ANOVA

followed by the Bonferroni post-hoc test. Comparisons between 2 groups were made using the unpaired t-test. For survival analysis, a Kaplan-Meier survival curve was generated, and log-rank statistics test was rendered. For all the statistical analyses, significance was accepted at $P<0.05$.

Results

1. Efficacy of selected shRNA TTN in suppressing the level of mRNA-TTN in vivo

The efficacy of AAV9-ShTTN in downregulating TTN mRNA in vivo was assessed in mice at different ages (adult and neonatal).
In CD1 pups, AAV9-ShTTN or a control vector was injected intraperitoneally (n°3 per group) at day 0, and animals were euthanized at day 6. mRNA analysis was performed in total heart, confirming strong reduction in TTN mRNA in AAV9-shTTN treated pups in respect to the control group (figure 1, panel 1a).

In adult mice (CD1 12 weeks old female, n°6 per group), AAV9-ShTTN or control vector were administered by intravenous tail injection and mice were euthanized at 7, 14 and 21 days (n°2 x group x each time point). Adult CMs were isolated from the whole heart with a Langendorff-free method and TTN mRNA levels were assessed. As shown in Figure 1, panel 1b, our AAV9-shTTN showed great efficacy in downregulating target mRNA at all time points.

2. In vivo cardiac functional effect of shRNA TTN

We hence evaluated the in vivo functional effect of AAV9-shTTN in mice.
For this purpose, we injected AAV9-shTTN or a control vector in CD1 pups at day 0 (30 mcl of 1×10^{13} vg/animal, n°9 per group), and evaluated by echocardiography at different time points (10 days and 3 month) (figure 2, panel 2a). Four treated animals died of severe heart failure (HF) with DCM between day 10 and day 15 (figure 2, panel 2b). Survivors showed markedly dilated phenotype with depressed LV function (figure 2, panel 2 c-e and table 1). Notably, treated animals showed a trend toward LV mass reduction in respect to controls (Heart weight in g/tibia length in mm ratio: 0.0070 vs 0.0085, echocardiographic LV mass in mg 82 vs 95 mg) (table 1).

In adult mice (CD1 12 weeks old female, n° 8 per group), AAV9-shTTN or a control vector (150 mcl of 1×10^{13} vg/animal) were injected intravenously, and the animals were evaluated by echocardiography at different time points (3 weeks and 5 weeks) (figure 3, panel 3a). After 3 weeks, there was any difference in term of function and dimension of the LV between the treated and the control animals. Three treated animals died with a post-mortem hypertrophic phenotype between the first and the second time point (figure 3, panel 3b). Survivors at 5 weeks showed markedly hypertrophic cardiac phenotype with preserved or mildly reduced LV function (figure 3, panel 3c-e and table 2). Notably, treated animals showed a significantly increase of LV wall

thickness and LV mass in respect to controls (Heart weight in g/tibia length in mm ratio: 0.0079 vs 0.0064, echocardiographic LV mass in mg: 149 vs 91 mg) and an important LV diastolic disfunction (left atrial area in mm^2: 6±1.4 vs 2.6±0.4; $p<0.05$) (table 2).

3. In vivo tissue and cellular characterization after shTTN injection

To assess if the different cardiac phenotype induced by AAV9-shTTN in pups and adult mice *in vivo* was related to altered CM turnover, we checked CM proliferation, dimensions, and apoptosis in these models.

In neonatal mice euthanized at day 3 analysis of EdU incorporation revealed non-significant variation or a mild decrease in the number of EdU positive CMs in hearts treated with AAV9-shTTN, in respect to control animals (8.9% vs 16.7% in treated versus control pups, $p<0.05$) (figure 4, panel 4a-b). Furthermore, CM cross sectional area was significantly reduced in pups that received AAV9-shTTN at day 10 (WGA fiber area: 87±38 μm^2 vs 121±23 μm2 in treated vs control pups, $p<0.05$) (figure 4, panel 4c). While apoptosis was not significantly increased in treated animals when assessed with TUNEL assay (0,5% vs 0,3% of TUNEL positive cells, p=ns) (figure 4, panel 4e). When we assessed CM cross sectional area in survived pups with DCM at 3 months, we found that CMs showed a compensatory cellular hypertrophy (WGA fiber area: 626±234 μm^2 vs 457±134 μm2 in treated vs control animal $p<0.05$) (figure 4, panel 4d).

Conversely, analysis of EdU incorporation in adult mice revealed a marked increase in the number of EdU positive CMs in hearts treated with AAV9-shTTN in respect to controls animal (1.67% vs 0.09% in treated versus control pups, $p<0.05$) (figure 5, panel 5a-b). CM cross sectional area was significantly reduced in adults that received AAV9-shTTN, with WGA fiber median area of 231 (IQR 176-298) μm^2 vs 299 (IQR 255-356) μm2 observed in controls ($p<0.05$) (figure 5, panel 5c). Also, in treated adult mice, there was not an increase of fibrosis or inflammatory infiltration compared to the control's hearts by a histological evaluation (figure 5, panel 5d).

Since it is known that EdU incorporation in CM's nuclei could also be due to events unrelated to cell proliferation (e.g. binucleation), we decided to use an alternative tool for the evaluation of CM proliferation by employing a fluorescent genetic reporter model: the Cyclin-B- CRE Z/EG mouse model. These animals express GFP fluorescent protein only after recombination by Cre recombinase, which is under the promoter of Cyclin B, as a marker of S/G2/M transition. This model allows to track mitotic events through GFP detection.

Adult Cyclin-B- CRE Z/EG mouse were subjected to the same experimental model: AAV9-shTTN treated animals also showed marked increase in GFP positive CMs in hearts compared to controls animal (figure 6, panel 6b). Treated animals showed increased LV wall thickness and LV mass compared with controls, associated with LV dilatation and dysfunction (LVEDV: 110 vs 67 ml in shTTN vs control vector; LVEF:33±5% vs 62±4% in shTTN vs control vector) (figure 6, panel 6c).

4. **Functional effect of TTN downregulation in a pathological mouse model of myocardial injury induced by myocardial infarction**

The same results were also obtained in the adult CD1 model with MI induced by LAD ligation (Figure 7). On the same day as the MI, mice received intravenous administration of AAV9-shTTN or a control vector (150 mcl of 1×1013 vg/animal, 3 per group). After 2 weeks from the MI, we conducted serial injections of EdU, and the mice were sacrificed after 4 weeks. Cardiac function was assessed through echocardiographic analysis both on the day of infarction and after the 4-week period. Notably, starting from echocardiographic data comparable to the baseline, infarcted mice that received AAV9-shTTN exhibited lower reduction in LVEF (at the baseline= LVEF:34±5% vs 32±3% in shTTN vs control vector; after 4 weeks= LVEF:34±7% vs 23±2%), along with a slight increase in IVSd and LVPWd thickness (at the baseline= IVSd:0.62±0.05 mm vs 0.61±0.12 mm and LVPWd: 0.45±0.07 mm vs 0.42±0.06 mm in shTTN vs control vector; after 4 weeks= IVSd: 0.78±0.02 mm vs 0.43±0.11 mm and LVPWd: 0.61±0.01 mm vs 0.38±0.07 mm in shTTN vs control vector), at the 4-week echocardiography. Furthermore, immunofluorescence staining for EdU incorporation revealed a significant increase in the number of EdU-positive CMs in the hearts treated with AAV9-shTTN, in comparison to the control animals (qualitative evaluation). These results suggest that TTN downregulation also in post-MI hearts promotes CM proliferation.

5. **In vitro cellular and proliferation characterization after TTN downregulation**

In the context of this study, we sought to investigate the impact of a siRNA targeting TTN on in vitro CM proliferation (Figure 8).

Employing three technical replicates for each group, we exposed neonatal CMs (P0 pups) to siRNA TTN pool, which was then compared to control groups, including those subjected to lipids only and a nto-targeting siRNA (NT siRNA). Furthermore, we examined the effects of siRNA targeting other sarcomeric genes, specifically MYH7 and MYBPC3. At day 4, following a 20-hour Edu pulse, the cells were fixed and subjected to a detailed immunostaining procedure for Edu. Notably, the cardiomyocytes treated with siRNA TTN exhibited a significant increase in proliferation, exceeding

5%, in contrast to both the control groups and those treated with siRNA against other sarcomeric genes (Figure 8A-B). Subsequently, we endeavoured to replicate these experiments using adult CMs obtained through Langendorff perfusion. However, it was observed that these adult CMs had a considerably shorter lifespan in vitro, with a maximum viability of only 2-3 days. In an attempt to extend our findings to the adult cardiac context, Langendorff-perfused hearts from adult CD1 mice were injected with shTTN or control vector along with Edu 48h pulse, 30 days prior to the experiment. Regrettably, this approach yielded only normal adult cardiomyocytes with intact sarcomeric structures and no detectable Edu-positive cells (Figure 8C).

6. TTN downregulation, sarcomeric disarray and CM proliferation

This study delved into an extensive analysis of sarcomeric organization, establishing a profound connection with the downregulation of the TTN gene through the application of siRNA and shRNA in both neonatal and adult CMs. To accomplish this, specific antibodies were employed for the immunostaining of sarcomeric components, including TTN, troponin, and alpha-actin. In addition, we scrutinized different TTN isoforms using specific antibodies, primarily focusing on N2BA and N2B. Indeed, it is well established that an important isoform switch is occurring after the first week of life in mammals, thus we wondered if TTN silencing with siRNA was affecting differently the two isoforms.

Neonatal CMs treated with siRNA targeting TTN revealed a striking disarray and disorganization of the normally organized and parallel sarcomeres seen in control groups (Figure 9A). Notably, the CMs displaying more pronounced sarcomeric disarray were correlated with a higher degree of EdU incorporation, suggesting that cells with diminished TTN levels were more inclined to initiate proliferation (Figure 9B).

Furthermore, we sought to investigate the potential variations in the downregulation of TTN isoforms as an explanatory factor for differences in CM proliferation observed in vivo. Our assessments encompassed both in vitro immunostaining of siRNA-treated cardiomyocytes and RT-PCR analysis of RNA extracted from the hearts of neonatal pups treated with AAV9-shRNA for TTN and sacrificed at P10. These investigations indicated a consistent downregulation of both TTN isoforms (Figure 9C-D).

Similarly, immunostaining of TTN in the heart tissue of adult mice treated with AAV9-shRNA for TTN and administered Edu demonstrated a significant disruption in CM organization. This disruption manifested as varying cell dimensions, with some cells retaining a well-organized sarcomeric structure, while others were smaller, marked by alpha-actinin positivity (characteristic

of CMs) but exhibited markedly reduced or absent TTN staining (Figure 10A). Intriguingly, these same cells were associated with a positive incorporation of EdU, validating the findings observed in the neonatal in vitro model, indicating that CMs with sarcomeric disarray and TTN downregulation had an enhanced propensity for proliferation. Moreover, RT-PCR analysis of RNA extracted from these hearts revealed a more pronounced impact on the downregulation of the N2B isoform, which is notably the more predominant isoform in adult hearts (Figure 10B). These findings collectively highlight the profound influence of TTN downregulation on sarcomeric disarray and its correlation with increased cardiomyocyte proliferation in both neonatal and adult cardiac contexts.

7. Role of TTN downregulation in proliferation and mechanical contraction of neonatal CM in engineering heart tissue (EHT)

To further confirm shTTN-mediated sarcomeric disarray and insufficiency, contractility was assessed with EHT. Primary neonatal rat CMs were extracted and cultured in EHT scaffolds. On the same day, CMs were infected with AAV6-shTTN or a control vector, and EdU was introduced 48 h prior to each designated timepoint. EHTs were incubated in a humidified cell culture incubator at 37°C with 7% CO2, with media changes occurring every other day. Spontaneous beating measurements of the EHTs were recorded at 1 week and 2 weeks in culture during the moment of maximum frequency contraction (burst). Immunofluorescence assays for EdU reaction were performed after both 1 and 2 weeks. The EHT force evaluation revealed a reduction in contractile force in the treated condition compared to controls (Figure 11). This difference was more pronounced at 1 week in culture (reduction >50%), while after 2 weeks, the contraction force of AAV6-shTTN EHTs mildly increased. These findings demonstrate that even in an in vitro 3D model employing neonatal CMs, TTN downregulation leads to a decrease in CM contractile force.

8. RNA-Seq in adult and neonatal mouse model, preliminary analysis

To deeply unravel the underlying mechanisms driving the distinct phenotypic outcomes following shTTN administration at different ages, we conducted comprehensive RNA-sequencing analyses. Neonatal mice received AVV-9 shTTN or a control vector at postnatal day 0 (P0) and were sacrificed at P4 or P8, while adult animals were administered the same constructs at 10 weeks of age and sacrificed at 14 and 35 days (Figure 12). Prior to harvest, echocardiography confirmed the anticipated phenotypes. Multiple transcriptomic comparisons were carried out among different age-matched groups and within the same age group with various time points (Figure 12A).

Initial transcriptomic analysis indicated that mice formed distinct clusters based on age and the treatment they received, illustrating robust differences in gene expression profiles (Figure 12B). Furthermore, a progressive increase of TTN mRNA transcript with age was also confirmed.

In summary, hearts from P4 mice injected with shTTN exhibited a more immature transcriptomic profile in comparison to control mice, marked by the upregulation of embryonic genes such as NANOG and SOX4. These findings suggest that TTN downregulation delays the cardiac differentiation process, maintaining a high expression of embryonic genes until day 4 of life. This delay may hinder CMs from developing a mature sarcomeric structure essential for adapting to the physiological increase in cardiac load shortly after birth. Ultimately, this deficit results in LV dilatation and dysfunction, mimicking a DCM phenotype.
This was supported by the downregulation, in treated animals, of transcripts involved in the formation of sarcomere (Figure 12C), such as MYL2 and MEF2c.

In contrast, adult mice treated with shTTN and sacrificed at 14 and 35 days exhibited an expression profile characteristic of highly proliferative tissues, marked by the upregulation of specific markers like SPRR1, CHODL, CTHRC1, and XIRP2, compared to control groups. Xirp2 was particularly relevant in our analysis to recent association of this protein with the upstream regulator of the YAP pathway. This indication was further accompanied by a notable activation of the YAP pathway (highlighted by the upregulation of the Yap related protein: TEAD, TAZ, and CCN1-2) and the PI3K-Akt pathway (PI3K and HB-EGF). This was accompanied by a notable upregulation of YAP target genes (TEAD, TAZ, and CCN1-2) and of the PI3K-Akt pathway (PI3K and HB-EGF transcripts).

These results align with our earlier hypothesis, which implicates sarcomere disassembly as a primary driver of cardiomyocyte proliferation.

Furthermore, when analyzing actin polymerization function, the transcriptome of adult treated mice suggests an upregulation of pathways supporting cytoskeletal reorganization conducive to cardiomyocyte proliferation. Factors upstream of actin polymerization (FHOD3, PI3K) and microtubule stabilizers (SPECC1) were highly represented in the 35-day mice treated with shRNA for TTN. This was coupled with the reactivation of GATA4 and MAPK pathways, possibly suggesting a dedifferentiation of these cardiomyocytes to embryonic stages, mirroring the trends observed in the younger cohort of treated mice.

Discussion

We initiated this study with the primary objective of delving deeper into the underlying mechanisms through which heterozygous TTNtvs variants could give rise to the characteristic phenotypic manifestations of DCM. Historically, the prevailing hypothesis had centered on TTN haploinsufficiency as the primary causative mechanism for elucidating the pathogenic processes associated with these variants. However, recent literature has introduced novel perspectives.

Despite the frequent occurrence of heterozygous TTNtvs in DCM cases, a comprehensive understanding of the precise mechanistic pathways by which they precipitate the disease remains elusive. Recent studies have suggested that both TTN haploinsufficiency and the cytotoxicity arising from aggregated truncated TTN proteins collectively contribute to the pathogenesis of DCM. Arany and colleagues (78) employed advanced techniques, including electrophoretic gels, allelic phasing, and proteomic mass spectrometry, to scrutinize 184 explanted post-transplantation DCM hearts. Their findings indicated that truncated TTN proteins were quantitatively detectable in the myocardium of DCM patients harbouring TTNtvs. Furthermore, these hearts exhibited a reduced total content of normal TTN protein compared to DCM hearts devoid of TTNtvs, suggestive of a state of titin haploinsufficiency. A parallel investigation by Linke and colleagues(79) yielded congruent results. Examination of myocardial tissue samples from 113 end-stage DCM patients, encompassing 22 individuals with heterozygous TTNtvs, revealed a diminished content of normal titin protein in TTNtvs-affected hearts, in comparison to DCM hearts and non-failing hearts. This reduction was associated with a 31% decrease in sarcomere content, which elucidated the weakened contractile force observed in hearts with TTNtvs variants. Notably, TTNtvs-affected hearts exhibited a stable expression of truncated titin protein, which aggregated intracellularly. The accrual of truncated TTN protein in these aggregates may exert cytotoxic effects, impeding protein quality control mechanisms, and potentially contributing to a 'poison-peptide' mechanism underlying DCM pathophysiology.

On the other hand, Eulalio and colleagues demonstrate for the first time that CM proliferation could be stimulated through the exogenous administration of miRNAs and, most pertinently, that such treatment can restore cardiac mass and promote functional recovery after myocardial infarction in adult animals. The marked proliferative effect exerted by these miRNAs likely ensues as the sum of their effects on multiple, individual genes, among which TTN was notably identified, implying that downregulation of TTN could potentially induce CM proliferation. Consequently, the initial inquiry of our study was framed around the exploration of whether an uncharted mechanistic avenue,

involving an alteration of CM proliferation, might underlie the pathogenesis of TTNtvs variants in the development of DCM.

However, what we obtain and understand with this study was probably something different but still very interesting from a physiological point of view.

First and foremost, our research strategy involved the development of a cardiac model in which TTN was downregulated through the incorporation of siRNA/shRNA delivered via AAV. This methodological approach warrants mention, as it deviates from the natural occurrence in human subjects carrying TTNtv, wherein the mutation is present in all cardiac cells in heterozygosity. In our model, siRNA interfering could potentially lead to a complete stop of TTN mRNA translation, leading to increased haploinsufficiency in respect to human disease. In our model, however, there is a limitation in terms of the cellular penetration of this genetic construct, particularly notable in the adult mouse model compared to neonatal mice. Consequently, not all CM within our model exhibited a comprehensive downregulation of TTN.

Nevertheless, subsequent to the successful achievement of a downregulation exceeding 50%, the primary focus of our study was to investigate the effects of TTN downregulation on the cardiac phenotype, particularly in relation to CM proliferation. In line with this objective, we decided to administer our molecular constructs to animal models at different developmental stages, for several compelling reasons:

1) Differential Role of Sarcomere and TTN Across Developmental Stages: The role of the sarcomere, and consequently TTN, varies at different stages of development. In neonates, the sarcomeric structure is more elastic, prone to proliferation, maturation and hypertrophy. These capacities persist until the early days of life. Conversely, in adults, sarcomere structure is highly specialized anc complex, with absence of CM proliferation.
2) Manifestation of TTNtv Cardiomyopathy: TTNtv cardiomyopathy typically manifests in adulthood, although genetic variants is germinal.
3) Age-Dependent Transcription of TTN Isoforms: Importantly, the transcription of TTN isoforms varies quantitatively at different life stages.

In the neonatal model, our observations yielded a phenotype that, in echocardiography, closely resembled the human model of TTNtv-related DCM. The LV of neonatal mice treated with shTTN, indeed, approximately ten days post-injection, exhibited severe dilatation and dysfunction, mirroring the LV of human DCM patients. Interestingly, the DCM phenotype in this model

displayed variability, ranging from severe cases with biventricular dilation and high mortality between days 10 and 14, to milder forms that survived into adulthood with mild LV dilation and dysfunction. This suggests a possible linear dose-effect relationship. It is worth noting that the technique of intraperitoneal injection in neonatal pups is inherently subject to slight but potentially significant variations in the injected volume.

Distinguishing our neonatal model from human TTNtv-related DCM is the reduction in TTN production, which is not compensated by the normal production of TTN from the unaffected chromosome as in heterozygous TTNtv carriers. This likely leads to a significant sarcomeric disarray within the CMs. In neonatal days, when hemodynamic changes occur, such as a substantial increase in heart preload and output, the standard adaptation capacity of these cells, in which TTN plays a crucial role in, is impaired. This impairment likely leads to decreased myofibrillar maturation and stiffness in CM, which are unable to counterbalance hemodynamic stresses and so underlies the observed LV changes during this process.

Furthermore, in this context, even though there was an upregulation of certain pro-proliferative genes at 8 days post shTTN injection (XIRP2, TEAD, CCND2), there was not a strong increase in CM proliferation rate. It has to be underlined that neonatal heart, until day 8 post-birth, are physiologically proliferating. During this period, indeed, the mammalian heart is characterized by a rapid growth by means of proliferation, polyploidization and progressive hypertrophy and maturation of CM. Our hypothesis in this context is that the impact of TTN downregulation on the proliferation rate could not be properly addressed in this model: CMs of pups treated with shTTN are physiologically proliferating, but also experiencing a delay in the normal maturation process typical for their age. This delay could in turn potentially modulate CM proliferation rate, but the absence of mature sarcomeric structures leads to severe systolic dysfunction, HF, and death, thus rendering unsuitable this *in-vivo* model for our purposes. Our data also showing the downregulation of both TTN isoforms, halting the typical shift towards maturation which involves an increase in the N2B isoform, is in line with this hypothesis.

This suggests that alteration of CM proliferation is probably not a causative mechanism for DCM development, whereas haploinsufficiency appears to be a more prominent factor.
Moreover, our utilization of shTTN did not yield the production of abnormal proteins, thereby contradicting the theory of a "poison peptide" mechanism in the neonatal mouse model. However, it's important to note that this does not rule out the possibility that some TTNtv could still act through both mechanisms, or that some predominantly utilize the "poison peptide" mechanism.

The neonatal model results were not entirely unexpected, and while we were progressing with these experiments, Jiang and colleagues(80) concurrently reported similar findings in a neonatal mouse model treated with shTTN, thus confirming the likeness of their results to our observations. Remarkably, neither study detected any alterations in proliferation capacity, despite a slight increase in the transcription of Ccnd1 and Ccnd2, which are cyclin proteins associated with mitosis.

The truly remarkable and unexpected findings emerged from our experiments conducted with the adult mouse *in vivo* model. Treatment of adult mice with AAV9-shTTN yielded an entirely distinct myocardial phenotype that deviated significantly from DCM, with no known human disease counterpart identified to date. Specifically, the administration of shTTN via intravenous injection in adult mice resulted in a substantial increase in biventricular wall thickness, alongside preserved or only minimally impaired LV systolic function and severe diastolic dysfunction, as preliminarily estimated by left atrium dilation. Following these changes, both the left and right ventricular chambers were effectively obliterated by these extremely hypertrophic LV walls. Moreover, the severity of this phenotype was found to be variable, directly correlating with the quantity of AAV9-shTTN administered.

Notably, despite a significant increase in wall thickness and LV mass, the cross-sectional area of CMs was not enlarged when compared to controls. Rather, it exhibited an abnormal distribution characterized by a high number of small CMs coexisting with normal-sized cells. This could support the evidence from EdU incorporation assays and the Z/EG model, strongly suggesting that the tissue generated was not merely hypertrophic but hyperplastic. This tissue displayed multiple CMs that tested positive for EdU incorporation or GFP expression in Z/EG mice, indicative of an actively proliferative tissue compared to control adult mice. This study achieved an increase in CM proliferation rate, measured at 1.67% versus the 0.09% observed in controls, and notably, there were no indications of fibrosis deposition, a characteristic feature of hypertrophic cardiomyopathy in humans.

Even more astonishing was the observation that the administration of shTTN in adult mice immediately after the induction of a severe MI through LAD ligation had a protective effect on the LV, preventing the adverse reverse remodelling typical of this pathological condition. Typically, the MI-surrounding area in animal models exhibits a slight induction of CM proliferation, which might serve as a protective but insufficient mechanism adopted by the heart to mitigate ischemic damage, as suggested by previous research (81). However, this intrinsic attempt at repair is usually limited and does not reach clinical significance. In contrast, the application of shTTN, with its capacity to effectively induce proliferation, significantly increased the thickness of the preserved LV. This

preservation occurred without complete myocardial replacement of the necrotic area, but it effectively maintained the dimensions and functionality of the LV. In the control group, these parameters worsened, as demonstrated by echocardiographic evaluations conducted four weeks post-MI.

Confocal microscopy of in vivo proliferating CMs revealed that Edu + CM stained negative for TTN, showing de-structured sarcomeres. We acknowledge that our AAV9-shTTN construct does not allow to track and identify infected cells. However, these staining represents our strongest evidence associating *in vivo* CM proliferation with downregulation of TTN.

We hence proceed in establishing an *in-vitro* model to dissect the molecular mechanisms behind this association: while prolonged in vitro culture of adult CMs was technically challenging due to their limited viability, we opted to experiment with neonatal CMs, and this approach proved highly relevant to our study.
Although *in-vivo* neonatal CMs do not represent a suitable model due to hemodynamic conditions, *in-vitro* conditions proved to be a valuable tool under standardized condition. Histological analysis of these neonatal CMs, conducted four days after they were treated with TTN-targeting siRNA and subjected to a pulse of EdU, revealed a significant sarcomeric disarray in many CMs. These cells displayed a deformed, more circular shape, primarily attributed to the pronounced disruption of sarcomeres, notably linked to the near absence of Titin.

Furthermore, the CMs that exhibited more profound disarray and lower TTN expression were the same ones with higher levels of EdU incorporation. This suggested that TTN and the well-structured, stiffer sarcomere might play a role in restraining CM proliferation. The downregulation and disarray of TTN appeared to trigger the reactivation of certain primordial, pro-proliferative pathways. The transcriptome analysis of these highly proliferative hearts, induced through shTTN treatment, also unveiled a significant upregulation of the YAP, PI3K-Akt, MAPK, and GATA4 pathways, indicative of a process akin to dedifferentiation of these CMs to embryonic stages.

To evaluate the contractile function of these CMs after the disruption of their sarcomeric structures, yet with the concurrent highly proliferative activation induced by shTTN, we employed EHTs in a 3D in vitro culture. These EHTs allowed us to assess the strength generated by these CMs, revealing a notable inefficiency in generating contractile forces.

In summary, we here show that TTN downregulation in CM leads to proliferation in vivo, mediated by multiple pathways including Hippo and PI3K-Akt. Multiple questions remain to be solved. If observation from histological, in vitro and transcriptomic data are consistent, the link(s) between

absence of TTN and proliferation are not elucidated. Titin seems to represent an inhibitor of proliferation process: CM lacking Titin, as other un-differentiated cells, intrinsically proliferate, until a mature sarcomeric structure stops this process.

In conclusion, our study has unveiled a significant and unexpected revelation – the pro-proliferative effect of sarcomere disruption for the first time. This discovery has become a central point of focus, transcending the initial scope of our investigation into DCM caused by heterozygous TTNtvs. While the precise DCM link remains inconclusive, the capacity of sarcomere disarray to stimulate CM proliferation stands as a remarkable observation.

Furthermore, despite the increased proliferative capacity observed in CMs, this process, if not controlled, is deleterious. The disorganized tissue structure induced by TTN downregulation in the adult heart presents challenges when considering them as a potential therapy for myocardial regeneration. These findings emphasize the need for further research to fully comprehend the implications of sarcomere deconstruction and the potential applications of CM proliferation in the context of cardiac regeneration.

References

1. Bicknell KA, Coxon CH, Brooks G. Can the cardiomyocyte cell cycle be reprogrammed? Vol. 42, Journal of Molecular and Cellular Cardiology. J Mol Cell Cardiol; 2007. p. 706–21.

2. Poss KD, Wilson LG, Keating MT. Heart regeneration in zebrafish. Science (80-). 2002 Dec 13;298(5601):2188–90.

3. Ali H, Braga L, Giacca M. Cardiac regeneration and remodelling of the cardiomyocyte cytoarchitecture. FEBS J. 2020;287(3):417–38.

4. Eulalio A, Mano M, Ferro MD, Zentilin L, Sinagra G, Zacchigna S, et al. Functional screening identifies miRNAs inducing cardiac regeneration. Nature. 2012 Dec 5;492(7429):376–81.

5. Herman DS, Lam L, Taylor MRG, Wang L, Teekakirikul P, Christodoulou D, et al. Truncations of Titin Causing Dilated Cardiomyopathy. N Engl J Med. 2012 Feb 16;366(7):619–28.

6. Ahuja P, Sdek P, MacLellan WR. Cardiac myocyte cell cycle control in development, disease, and regeneration [Internet]. Vol. 87, Physiological Reviews. Physiol Rev; 2007 [cited 2020 Oct 9]. p. 521–44. Available from: https://pubmed.ncbi.nlm.nih.gov/17429040/

7. Van Amerongen MJ, Engel FB. Features of cardiomyocyte proliferation and its potential for cardiac regeneration: Stem Cells Review Series. J Cell Mol Med [Internet]. 2008 Dec [cited 2020 Oct 9];12(6A):2233–44. Available from: /pmc/articles/PMC4514102/?report=abstract

8. Flink IL. Cell cycle reentry of ventricular and atrial cardiomyocytes and cells within the epicardium following amputation of the ventricular apex in the axolotl, Amblystoma mexicanum: Confocal microscopic immunofluorescent image analysis of bromodeoxyuridine-label. Anat Embryol (Berl). 2002;205(3):235–44.

9. Oberpriller JO, Oberpriller JC. Response of the adult newt ventricle to injury. J Exp Zool. 1974 Feb 1;187(2):249–59.

10. Oberpriller J, Oberpriller JC. MITOSIS IN ADULT NEWT VENTRICLE. J Cell Biol. 1971 May 5;49(2):560.

11. Jopling C, Sleep E, Raya M, Martí M, Raya A, Belmonte JCI. Zebrafish heart regeneration

occurs by cardiomyocyte dedifferentiation and proliferation. Nature [Internet]. 2010 Mar 25 [cited 2020 Oct 9];464(7288):606–9. Available from: https://pubmed.ncbi.nlm.nih.gov/20336145/

12. Kikuchi K, Holdway JE, Werdich AA, Anderson RM, Fang Y, Egnaczyk GF, et al. Primary contribution to zebrafish heart regeneration by gata4+ cardiomyocytes. Nature [Internet]. 2010 Mar 25 [cited 2020 Oct 9];464(7288):601–5. Available from: https://pubmed.ncbi.nlm.nih.gov/20336144/

13. González-Rosa JM, Sharpe M, Field D, Soonpaa MH, Field LJ, Burns CE, et al. Myocardial polyploidization creates a barrier to heart regeneration in zebrafish. Dev Cell. 2018 Feb 2;44(4):433.

14. Porrello ER, Mahmoud AI, Simpson E, Hill JA, Richardson JA, Olson EN, et al. Transient Regenerative Potential of the Neonatal Mouse Heart. Science. 2011 Feb 2;331(6020):1078.

15. Porrello ER, Mahmoud AI, Simpson E, Johnson BA, Grinsfelder D, Canseco D, et al. Regulation of neonatal and adult mammalian heart regeneration by the miR-15 family. Proc Natl Acad Sci U S A. 2013 Jan 2;110(1):187–92.

16. Soonpaa MH, Kim KK, Pajak L, Franklin M, Field LJ. Cardiomyocyte DNA synthesis and binucleation during murine development. https://doi.org/101152/ajpheart19962715H2183 [Internet]. 1996 [cited 2023 Oct 30];271(5 40-5). Available from: https://journals.physiology.org/doi/10.1152/ajpheart.1996.271.5.H2183

17. Soonpaa MH, Field LJ. Assessment of cardiomyocyte DNA synthesis in normal and injured adult mouse hearts. https://doi.org/101152/ajpheart19972721H220 [Internet]. 1997 [cited 2023 Oct 30];272(1 41-1). Available from: https://journals.physiology.org/doi/10.1152/ajpheart.1997.272.1.H220

18. Ye L, D'Agostino G, Loo SJ, Wang CX, Su LP, Tan SH, et al. Early Regenerative Capacity in the Porcine Heart. Circulation. 2018 Dec 11;138(24):2798–808.

19. Haubner BJ, Schneider J, Schweigmann U, Schuetz T, Dichtl W, Velik-Salchner C, et al. Functional Recovery of a Human Neonatal Heart after Severe Myocardial Infarction. Circ Res. 2016 Jan 22;118(2):216–21.

20. Bergmann O, Bhardwaj RD, Bernard S, Zdunek S, Barnabé-Heide F, Walsh S, et al. Evidence for cardiomyocyte renewal in humans. Science (80-) [Internet]. 2009 Apr 3 [cited 2020 Oct 8];324(5923):98–102. Available from: https://pubmed.ncbi.nlm.nih.gov/19342590/

21. Senyo SE, Steinhauser ML, Pizzimenti CL, Yang VK, Cai L, Wang M, et al. Mammalian heart renewal by pre-existing cardiomyocytes. Nature [Internet]. 2013 Jan 17 [cited 2020 Oct 8];493(7432):433–6. Available from: https://www.ncbi.nlm.nih.gov/pmc/articles/PMC3548046/

22. Soonpaa MH, Kim KK, Pajak L, Franklin M, Field LJ. Cardiomyocyte DNA synthesis and binucleation during murine development. Am J Physiol - Hear Circ Physiol [Internet]. 1996 [cited 2020 Oct 8];271(5 40-5). Available from: https://pubmed.ncbi.nlm.nih.gov/8945939/

23. Li F, Wang X, Capasso JM, Gerdes AM. Rapid transition of cardiac myocytes from hyperplasia to hypertrophy during postnatal development. J Mol Cell Cardiol. 1996;28(8):1737–46.

24. Mollova M, Bersell K, Walsh S, Savla J, Das LT, Park SY, et al. Cardiomyocyte proliferation contributes to heart growth in young humans. Proc Natl Acad Sci U S A [Internet]. 2013 Jan 22 [cited 2020 Oct 9];110(4):1446–51. Available from: https://pubmed.ncbi.nlm.nih.gov/23302686/

25. Alkass K, Panula J, Westman M, Wu T Di, Guerquin-Kern JL, Bergmann O. No Evidence for Cardiomyocyte Number Expansion in Preadolescent Mice. Cell. 2015 Nov 5;163(4):1026–36.

26. Olivetti G, Quaini F, Sala R, Lagrasta C, Corradi D, Bonacina E, et al. Acute myocardial infarction in humans is associated with activation of programmed myocyte cell death in the surviving portion of the heart. J Mol Cell Cardiol. 1996 Sep 1;28(9):2005–16.

27. Mollova M, Bersell K, Walsh S, Savla J, Das LT, Park SY, et al. Cardiomyocyte proliferation contributes to heart growth in young humans. Proc Natl Acad Sci U S A. 2013 Jan 22;110(4):1446–51.

28. Steinfeldt J, Becker R, Vergarajauregui S, Engel FB. Alternative splicing of pericentrin contributes to cell cycle control in cardiomyocytes. J Cardiovasc Dev Dis. 2021 Aug 1;8(8).

29. Sillibourne JE, Delaval B, Redick S, Sinha M, Doxsey SJ. Chromatin Remodeling Proteins Interact with Pericentrin to Regulate Centrosome Integrity. Mol Biol Cell. 2007 Sep;18(9):3667.

30. Kim J, Krishnaswami SR, Gleeson JG. CEP290 interacts with the centriolar satellite component PCM-1 and is required for Rab8 localization to the primary cilium. Hum Mol Genet. 2008 Dec 1;17(23):3796–805.

31. Leone M, Musa G, Engel FB. Cardiomyocyte binucleation is associated with aberrant mitotic microtubule distribution, mislocalization of RhoA and IQGAP3, as well as defective actomyosin ring anchorage and cleavage furrow ingression. Cardiovasc Res. 2018 Jul 1;114(8):1115–31.

32. Leone M, Engel FB. Advances in heart regeneration based on cardiomyocyte proliferation and regenerative potential of binucleated cardiomyocytes and polyploidization. Clin Sci. 2019 Jun 14;133(11):1229–53.

33. Heiden MGV, Cantley LC, Thompson CB. Understanding the Warburg Effect: The Metabolic Requirements of Cell Proliferation. Science (80-). 2009 May 22;324(5930):1029–33.

34. Ishihara T, Ban-Ishihara R, Maeda M, Matsunaga Y, Ichimura A, Kyogoku S, et al. Dynamics of Mitochondrial DNA Nucleoids Regulated by Mitochondrial Fission Is Essential for Maintenance of Homogeneously Active Mitochondria during Neonatal Heart Development. Mol Cell Biol. 2015 Jan 1;35(1):211–23.

35. Puente BN, Kimura W, Muralidhar SA, Moon J, Amatruda JF, Phelps KL, et al. The oxygen-rich postnatal environment induces cardiomyocyte cell-cycle arrest through DNA damage response. Cell. 2014 Apr 24;157(3):565–79.

36. Nakada Y, Canseco DC, Thet S, Abdisalaam S, Asaithamby A, Santos CX, et al. Hypoxia induces heart regeneration in adult mice. Nat 2017 5417636. 2016 Oct 31;541(7636):222–7.

37. Yahalom-Ronen Y, Rajchman D, Sarig R, Geiger B, Tzahor E. Reduced matrix rigidity promotes neonatal cardiomyocyte dedifferentiation, proliferation and clonal expansion. Elife. 2015 Aug 18;4(AUGUST2015).

38. Notari M, Ventura-Rubio A, Bedford-Guaus SJ, Jorba I, Mulero L, Navajas D, et al. The local microenvironment limits the regenerative potential of the mouse neonatal heart. Sci Adv. 2018 May 2;4(5).

39. Lavine KJ, Epelman S, Uchida K, Weber KJ, Nichols CG, Schilling JD, et al. Distinct macrophage lineages contribute to disparate patterns of cardiac recovery and remodeling in the neonatal and adult heart. Proc Natl Acad Sci U S A. 2014 Nov 11;111(45):16029–34.

40. Hirschy A, Schatzmann F, Ehler E, Perriard JC. Establishment of cardiac cytoarchitecture in the developing mouse heart. Dev Biol [Internet]. 2006 Jan 15 [cited 2020 Oct 9];289(2):430–41. Available from: https://pubmed.ncbi.nlm.nih.gov/16337936/

41. Lompre AM, Schwartz K, D'Albis A, Lacombe G, Van Thiem N, Swynghedauw B. Myosin isoenzyme redistribution in chronic heart overload. Nat 1979 2825734. 1979;282(5734):105–7.

42. Bouvagnet P, Mairhofer H, Leger JOC, Puech P, Leger JJ. Distribution pattern of alpha and beta myosin in normal and diseased human ventricular myocardium. Basic Res Cardiol. 1989 Jan;84(1):91–102.

43. Wilkinson JM, Grand RJA. Comparison of amino acid sequence of troponin I from different striated muscles. Nat 1978 2715640. 1978 Jan 1;271(5640):31–5.

44. Wheelwright M, Mikkila J, Bedada FB, Mandegar MA, Thompson BR, Metzger JM. Advancing physiological maturation in human induced pluripotent stem cell-derived cardiac muscle by gene editing an inducible adult troponin isoform switch. Stem Cells. 2020 Oct 1;38(10):1254–66.

45. Wiesmann F, Ruff J, Hiller KH, Rommel E, Haase A, Neubauer S. Developmental changes of cardiac function and mass assessed with MRI in neonatal, juvenile, and adult mice. Am J Physiol - Hear Circ Physiol. 2000;278(2 47-2).

46. Lahmers S, Wu Y, Call DR, Labeit S, Granzier H. Developmental control of titin isoform expression and passive stiffness in fetal and neonatal myocardium. Circ Res. 2004 Mar 5;94(4):505–13.

47. Canseco DC, Kimura W, Garg S, Mukherjee S, Bhattacharya S, Abdisalaam S, et al. Human ventricular unloading induces cardiomyocyte proliferation. J Am Coll Cardiol. 2015 Mar 10;65(9):892–900.

48. Lee YJ, Keng PC. Studying the effects of actin cytoskeletal destabilization on cell cycle by cofilin overexpression. Mol Biotechnol. 2005;31(1):1–10.

49. Pollard TD. Actin and Actin-Binding Proteins. Cold Spring Harb Perspect Biol. 2016 Aug 1;8(8).

50. Torrini C, Cubero RJ, Dirkx E, Braga L, Ali H, Prosdocimo G, et al. Common Regulatory Pathways Mediate Activity of MicroRNAs Inducing Cardiomyocyte Proliferation. Cell Rep. 2019 May 28;27(9):2759–2771.e5.

51. Miralles F, Posern G, Zaromytidou AI, Treisman R. Actin dynamics control SRF activity by regulation of its coactivator MAL. Cell. 2003 May 2;113(3):329–42.

52. Panciera T, Azzolin L, Cordenonsi M, Piccolo S. Mechanobiology of YAP and TAZ in physiology and disease. Nat Rev Mol Cell Biol 2017 1812. 2017 Sep 27;18(12):758–70.

53. Xin M, Kim Y, Sutherland LB, Qi X, McAnally J, Schwartz RJ, et al. Development: Regulation of insulin-like growth factor signaling by Yap governs cardiomyocyte proliferation and embryonic heart size. Sci Signal. 2011 Oct 25;4(196).

54. D'Uva G, Aharonov A, Lauriola M, Kain D, Yahalom-Ronen Y, Carvalho S, et al. ERBB2 triggers mammalian heart regeneration by promoting cardiomyocyte dedifferentiation and proliferation. Nat Cell Biol 2014 175. 2015 Apr 6;17(5):627–38.

55. Ahuja P, Perriard E, Perriard JC, Ehler E. Sequential myofibrillar breakdown accompanies mitotic division of mammalian cardiomyocytes [Internet]. Vol. 117, Journal of Cell Science. The Company of Biologists Ltd; 2004 [cited 2020 Oct 9]. p. 3295–306. Available from: https://jcs.biologists.org/content/117/15/3295

56. Sleep E, Boué S, Jopling C, Raya M, Raya Á, Belmonte JCI. Transcriptomics approach to investigate zebrafish heart regeneration. J Cardiovasc Med [Internet]. 2010 May [cited 2020 Oct 9];11(5):369–80. Available from: https://pubmed.ncbi.nlm.nih.gov/20179605/

57. Laube F, Heister M, Scholz C, Borchardt T, Braun T. Re-programming of newt cardiomyocytes is induced by tissue regeneration. J Cell Sci [Internet]. 2006 Nov 15 [cited 2020 Oct 9];119(22):4719–29. Available from: http://jcs.biologists.org/cgi/content/full/119/22/4719/DC1

58. Gregorio CC, Trombitás K, Centner T, Kolmerer B, Stier G, Kunke K, et al. The NH2 terminus of titin spans the Z-disc: Its interaction with a novel 19-kD ligand (T-cap) is required for sarcomeric integrity. J Cell Biol [Internet]. 1998 Nov 16 [cited 2020 Oct 9];143(4):1013–27. Available from: https://pubmed.ncbi.nlm.nih.gov/9817758/

59. Linke WA, Granzier H. A spring tale: New facts on titin elasticity [Internet]. Vol. 75, Biophysical Journal. Biophysical Society; 1998 [cited 2020 Oct 9]. p. 2613–4. Available from: https://www.ncbi.nlm.nih.gov/pmc/articles/PMC1299936/

60. Roberts AM, Ware JS, Herman DS, Schafer S, Baksi J, Bick AG, et al. Integrated allelic, transcriptional, and phenomic dissection of the cardiac effects of titin truncations in health and disease. Sci Transl Med [Internet]. 2015 Jan 14 [cited 2020 Oct 9];7(270):270ra6-270ra6. Available from: http://cardiodb.org/titin

61. Leinwand LA, Tardiff JC, Gregorio CC. Mutations in the sensitive giant titin result in a

broken heart. Circ Res [Internet]. 2012 Jul 6 [cited 2020 Oct 9];111(2):158–61. Available from: http://www.ncbi.nlm.nih.gov/pubmed/22773424

62. Lewinter MM, Granzier HL. Titin is a major human disease gene. Circulation [Internet]. 2013 Feb 26 [cited 2020 Oct 9];127(8):938–44. Available from: https://www.ahajournals.org/doi/10.1161/CIRCULATIONAHA.112.139717

63. Puchner EM, Alexandrovich A, Ay LK, Hensen U, Schäfer L V., Brandmeier B, et al. Mechanoenzymatics of titin kinase. Proc Natl Acad Sci U S A [Internet]. 2008 Sep 9 [cited 2020 Oct 9];105(36):13385–90. Available from: www.pnas.orgcgidoi10.1073pnas.0805034105

64. Elliott P, Andersson B, Arbustini E, Bilinska Z, Cecchi F, Charron P, et al. Classification of the cardiomyopathies: A position statement from the european society of cardiology working group on myocardial and pericardial diseases. Eur Heart J [Internet]. 2008 Jan [cited 2020 Oct 9];29(2):270–6. Available from: https://pubmed.ncbi.nlm.nih.gov/17916581/

65. Charron P, Arad M, Arbustini E, Basso C, Bilinska Z, Elliott P, et al. Genetic counselling and testing in cardiomyopathies: A position statement of the European Society of Cardiology Working Group on Myocardial and Pericardial Diseases [Internet]. Vol. 31, European Heart Journal. Eur Heart J; 2010 [cited 2020 Oct 9]. p. 2715–28. Available from: https://pubmed.ncbi.nlm.nih.gov/20823110/

66. Haas J, Frese KS, Peil B, Kloos W, Keller A, Nietsch R, et al. Atlas of the clinical genetics of human dilated cardiomyopathy [Internet]. Vol. 36, European Heart Journal. Oxford University Press; 2015 [cited 2020 Oct 9]. p. 1123–35. Available from: http://hgdownload.soe.ucsc.edu/goldenPath/hg19/

67. Walsh R, Thomson KL, Ware JS, Funke BH, Woodley J, McGuire KJ, et al. Reassessment of Mendelian gene pathogenicity using 7,855 cardiomyopathy cases and 60,706 reference samples. Genet Med. 2017 Feb 1;19(2):192–203.

68. Tayal U, Newsome S, Buchan R, Whiffin N, Halliday B, Lota A, et al. Phenotype and Clinical Outcomes of Titin Cardiomyopathy. J Am Coll Cardiol [Internet]. 2017 Oct 31 [cited 2020 Oct 9];70(18):2264–74. Available from: /pmc/articles/PMC5666113/?report=abstract

69. Ware JS, Cook SA. Role of titin in cardiomyopathy: From DNA variants to patient stratification [Internet]. Vol. 15, Nature Reviews Cardiology. Nature Publishing Group; 2018

[cited 2020 Oct 10]. p. 241–52. Available from: https://pubmed.ncbi.nlm.nih.gov/29238064/

70. Dal Ferro M, Severini GM, Gigli M, Mestroni L, Sinagra G. Genetics of Dilated Cardiomyopathy: Current Knowledge and Future Perspectives. In: Dilated Cardiomyopathy [Internet]. Springer International Publishing; 2019 [cited 2020 Oct 9]. p. 45–69. Available from: https://pubmed.ncbi.nlm.nih.gov/32091718/

71. Gerull B, Gramlich M, Atherton J, McNabb M, Trombitás K, Sasse-Klaassen S, et al. Mutations of TTN, encoding the giant muscle filament titin, cause familial dilated cardiomyopathy. Nat Genet [Internet]. 2002 [cited 2020 Oct 9];30(2):201–4. Available from: https://pubmed.ncbi.nlm.nih.gov/11788824/

72. Pugh TJ, Kelly MA, Gowrisankar S, Hynes E, Seidman MA, Baxter SM, et al. The landscape of genetic variation in dilated cardiomyopathy as surveyed by clinical DNA sequencing. Genet Med [Internet]. 2014 [cited 2020 Oct 9];16(8):601–8. Available from: https://pubmed.ncbi.nlm.nih.gov/24503780/

73. Fatkin D, Lam L, Herman DS, Benson CC, Felkin LE, Barton PJR, et al. Titin truncating mutations: A rare cause of dilated cardiomyopathy in the young. Prog Pediatr Cardiol. 2016 Mar 1;40:41–5.

74. Verdonschot JAJ, Hazebroek MR, Derks KWJ, Barandiarán Aizpurua A, Merken JJ, Wang P, et al. Titin cardiomyopathy leads to altered mitochondrial energetics, increased fibrosis and long-term life-threatening arrhythmias. Eur Heart J [Internet]. 2018 Mar 7 [cited 2020 Oct 9];39(10):864–73. Available from: https://pubmed.ncbi.nlm.nih.gov/29377983/

75. Hinson JT, Chopra A, Nafissi N, Polacheck WJ, Benson CC, Swist S, et al. Titin mutations in iPS cells define sarcomere insufficiency as a cause of dilated cardiomyopathy. Science (80-) [Internet]. 2015 Aug 28 [cited 2020 Oct 10];349(6251):982–6. Available from: /pmc/articles/PMC4618316/?report=abstract

76. Ackers-Johnson M, Li PY, Holmes AP, O'Brien SM, Pavlovic D, Foo RS. A Simplified, Langendorff-Free Method for Concomitant Isolation of Viable Cardiac Myocytes and Nonmyocytes from the Adult Mouse Heart. Circ Res [Internet]. 2016 Sep 30 [cited 2020 Oct 10];119(8):909–20. Available from: https://www.ahajournals.org/doi/10.1161/CIRCRESAHA.116.309202

77. Zacchigna S, Paldino A, Falcão-Pires I, Daskalopoulos EP, Dal Ferro M, Vodret S, et al. Towards standardization of echocardiography for the evaluation of left ventricular function

in adult rodents: a position paper of the ESC Working Group on Myocardial Function. Cardiovasc Res [Internet]. 2020 May 4 [cited 2020 Oct 10];0:1–17. Available from: https://academic.oup.com/cardiovascres/advance-article/doi/10.1093/cvr/cvaa110/5828935

78. McAfee Q, Chen CY, Yang Y, Caporizzo MA, Morley M, Babu A, et al. Truncated titin proteins in dilated cardiomyopathy. Sci Transl Med. 2021 Nov 11;13(618):eabd7287.

79. Fomin A, Gärtner A, Cyganek L, Tiburcy M, Tuleta I, Wellers L, et al. Truncated titin proteins and titin haploinsufficiency are targets for functional recovery in human cardiomyopathy due to TTN mutations. Sci Transl Med. 2021 Nov 3;13(618):11.

80. Liao D, Chen W, Tan CY, Wong JX, Chan PS, Tan LW, et al. Upregulation of Yy1 Suppresses Dilated Cardiomyopathy caused by Ttn insufficiency. Sci Reports 2019 91. 2019 Nov 8;9(1):1–12.

81. Ntonio A, Eltrami PB, Rbanek OU, Ajstura AK, Hao -M In S, An Y, et al. Evidence That Human Cardiac Myocytes Divide after Myocardial Infarction. https://doi.org/101056/NEJM200106073442303. 2001 Jun 7;2(11):1248–9.

FIGURES:

Figure 1: downregulation of TTN mRNA in different setting. **A** pups' CMs in vivo; **B** adult mice' CMs in vivo.

Figure 2: DCM induced by shRNA TTN in CD1 pups. **A** schematic timeline of the main experimental steps; **B**. Kaplan-Meier survival curves of CD1 pups treated at p0 with AAV9-shTTN (red) or control vector (green) ; **C-D**. Echocardiographic parasternal B -mode imaging of long and short axis view of LV; **E**. (clockwise): LVAWd, LV mass, LVEDV, EF (Simpson), of treated vs controls pups at 3 months.

Figure 3: Hyperplastic cardiomyopathy in adult mice induced by shRNA TTN. **A.** schematic timeline of the main experimental steps; **B**. Kaplan-Meier survival curves of CD1 adult mice treated at 12 weeks with AAV9-shTTN (red) or control vector(green); **C-D**. Echocardiographic parasternal B -mode imaging of long and short axis view of LV; **E**. (clockwise): LVAWd, LV mass, LVEDV, EF (Simpson), of treated vs controls adults at 3 and 5 weeks post injection.

Figure 4: CM replication in pups. **A**. EdU and a-actinin staining of mice hearts injected with AAV9-shTTN or control vector; **B**. Percentage of proliferating CMs in mice hearts in treated compared to controls (manual count); **C**. TUNEL assay; **D**. CM cross sectional area in pups at day 10 and 90 days.

Figure 5: CM replication in adult mice. **A** EdU and a-actinin staining of adult mice hearts injected with AAV9shTTN or control vector; **B** Percentage of proliferating Cardiomyocytes in adult mice hearts in treated compared to controls (manual count); **C** CM cross sectional area in adults at week 5; **D** Haematoxylin-eosin stain.

Figure 6: Z/EG mice model **A.** schematic timeline of the main experimental steps; **B**. GFP and a-actinin staining of mice hearts injected with AAV9-shTTN or control vector **C**. Echocardiographic evaluetion: LVEDV, LVESV, LVDD, LVEF (Simpson), of treated vs controls adults at 30 days post injection.

Figure 7: Myocardial infarction (LAD ligation) mice model. **A.** schematic timeline of the main experimental steps; **B**. EdU and troponin staining of mice hearts injected with AAV9-shTTN or control vector **C**. Echocardiographic evaluetion: LVEDV, LVAWd, LVPWd, LVEF (Simpson), of treated vs controls adults at 30 days post injection.

Figure 8: In vitro CM proliferation. **A.** EdU and a-actinin staining of CM extracted from pups P0 and treated with siTTN or control vectors; **B**. Proliferation rate (EdU positive CMs) in vitro CMs compared

to controls; **C**. Titin and a-actinin staining of adult CMs extracted by Langendorff-free method at day 30 from AAV9shTTN and control vector injection.

Figure 9: In vitro CM disarray, TTN staining and proliferation. **A.** Titin and a-actinin staining of CM extracted from pups P0 and treated with siTTN or control vector; **B**. Titin and EdU staining of CM treated with siTTN to highlight CM proliferation in correlation with sarcomeric disarray; **C**. Titin (with antibodies specific for the two TTN isoforms-N2B and N2BA and a-actinin staining of CMs treated with siTTN or control vector and quantification of TTN antibodies intensity. **D.** RT-PCR of CMs extracted from pups treated with shTTN and shCTR – quantification of TTN isoforms.

Figure 10: In vivo adult CMs disarray. **A.** Titin, a-actinin and EdU staining of heart tissue of adult mice treated with shTTN compared to control – CM disarray in treated animals; **B**. RT-PCR of CMs extracted from adult mice treated with shTTN and shCTR – quantification of TTN isoforms.

Figure 11: Engineer heart tissue (EHT) model. **A.** schematic timeline of the main experimental steps; **B**. Percentage of proliferating CMs (EdU positive CMs) in treated EHT compared to controls; **C**. Contractile force assessment of treated EHT compared to controls.

Figure 12: Transcriptome analysis. **A.** schematic timeline of the main experimental steps; **B**. main differences in gene expression profiles between groups. **C.** Main variation in cytoskeletal and sarcomeric genes transcription.

TABLES:

Table 1: Echocardiographic data of DCM in pups, induced by TTN shRNA, compared to control mice.

Table 2: Echocardiographic data of Hyperplastic Cardiomyopathy in adult mice, induced by TTN shRNA, compared to control mice.

Figure 1

A)

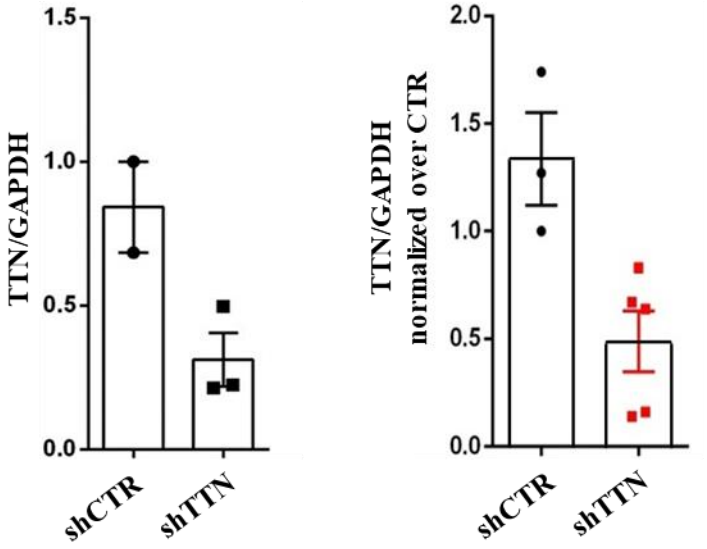
TTN/GAPDH
1.5
1.0
0.5
0.0
shCTR
shTTN
TTN/GAPDH
normalized over CTR
2.0
1.5
1.0
0.5
0.0
shCTR
shTTN

B)

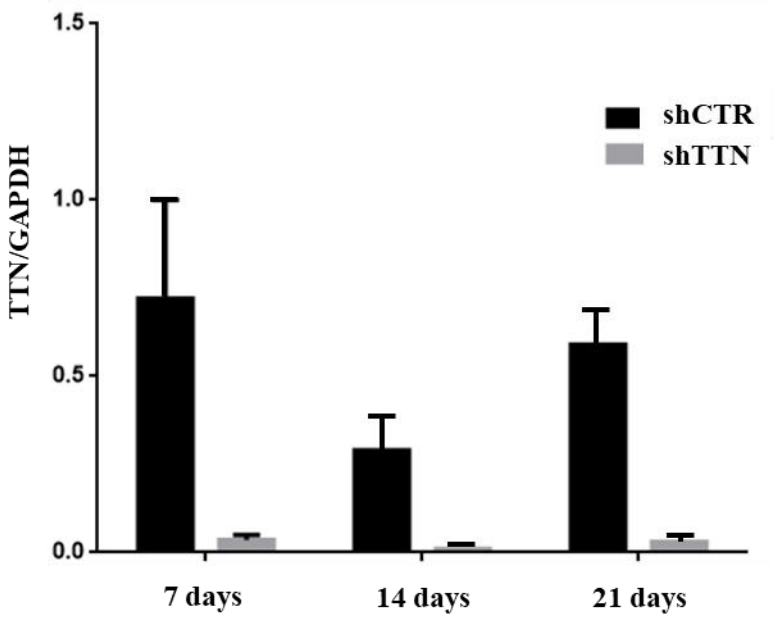
TTN/GAPDH
1.5
1.0
0.5
0.0
shCTR
shTTN
7 days
14 days
21 days

Figure 2

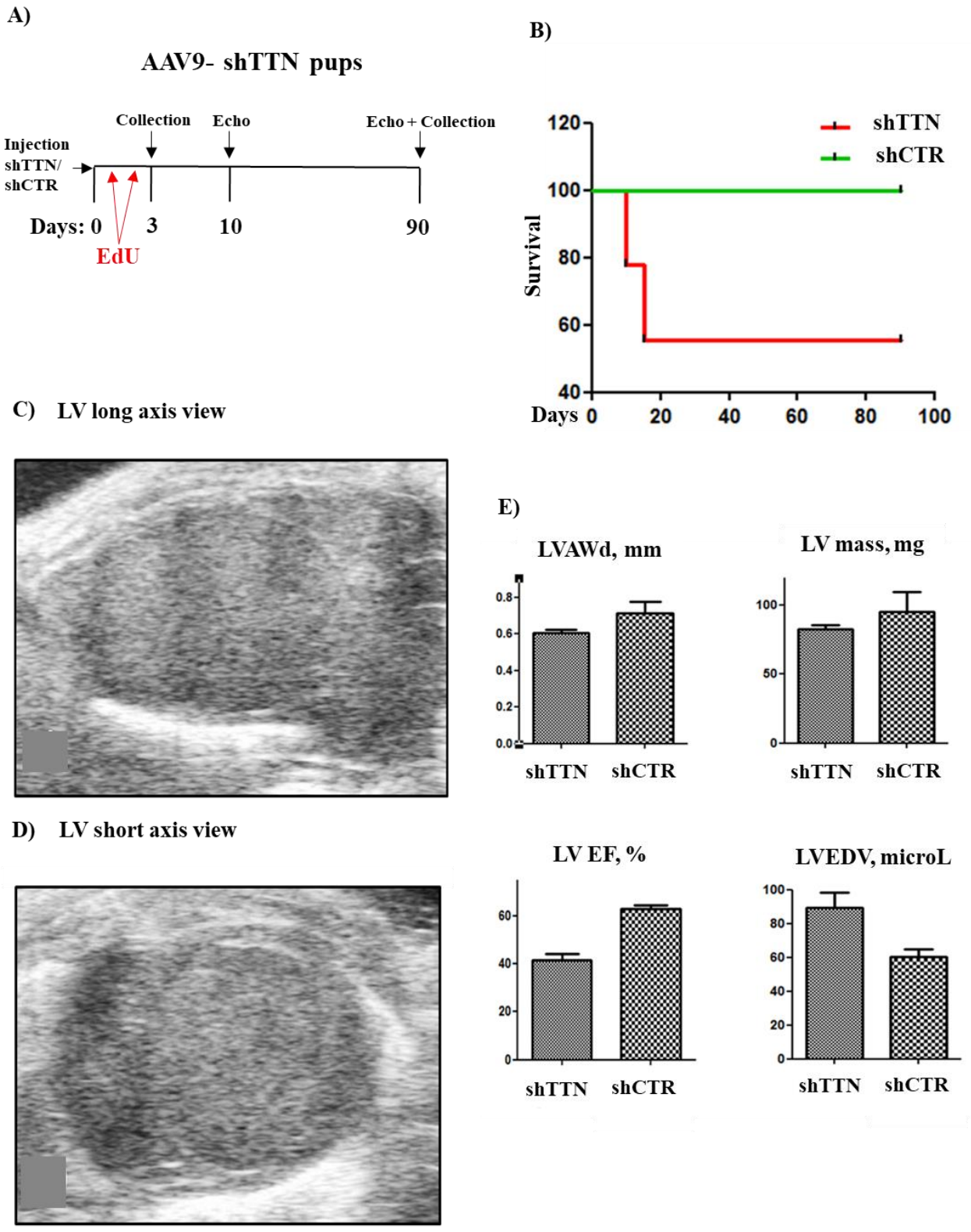
A)
AAV9- shTTN pups
Injection
shTTN/
shCTR
Collection
Echo
Echo + Collection
Days: 0
3
10
90
EdU
B)
shTTN
shCTR
Survival
120
100
80
60
40
Days 0
20
40
60
80
100
C) LV long axis view
D) LV short axis view
E)
LVAWd, mm
0.8
0.6
0.4
0.2
0.0
shTTN
shCTR
LV mass, mg
100
50
0
shTTN
shCTR
LV EF, %
60
40
20
0
shTTN
shCTR
LVEDV, microL
100
80
60
40
20
0
shTTN
shCTR

Figure 3

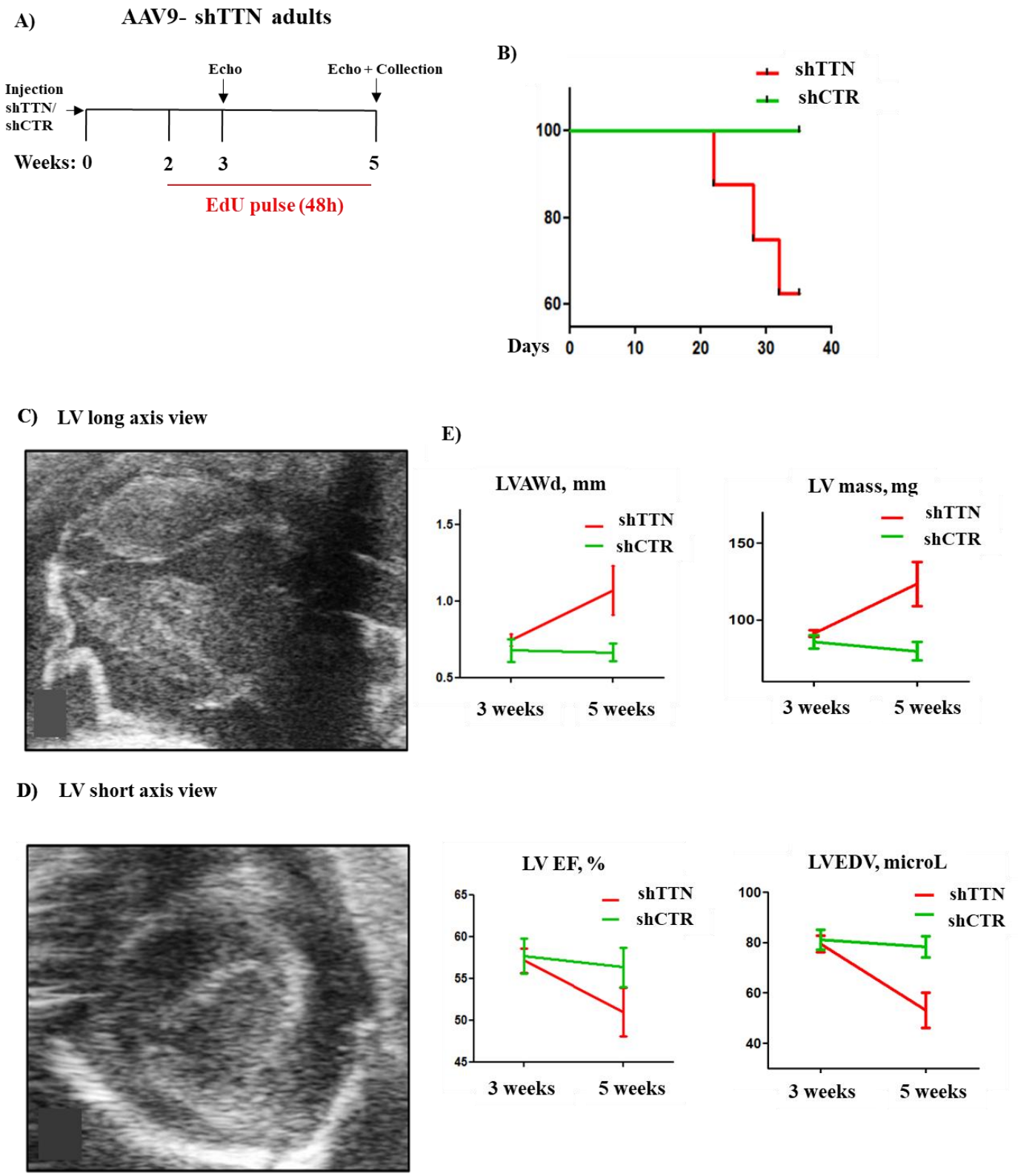
A)
AAV9- shTTN adults
Injection
shTTN/
shCTR
Echo
Echo + Collection
Weeks: 0
2
3
5
EdU pulse (48h)
B)
shTTN
shCTR
100
80
60
Days 0
10
20
30
40
C) LV long axis view
D) LV short axis view
E)
LVAWd, mm
shTTN
shCTR
1.5
1.0
0.5
3 weeks
5 weeks
LV mass, mg
shTTN
shCTR
150
100
3 weeks
5 weeks
LV EF, %
shTTN
shCTR
65
60
55
50
45
3 weeks
5 weeks
LVEDV, microL
shTTN
shCTR
100
80
60
40
3 weeks
5 weeks

Figure 4

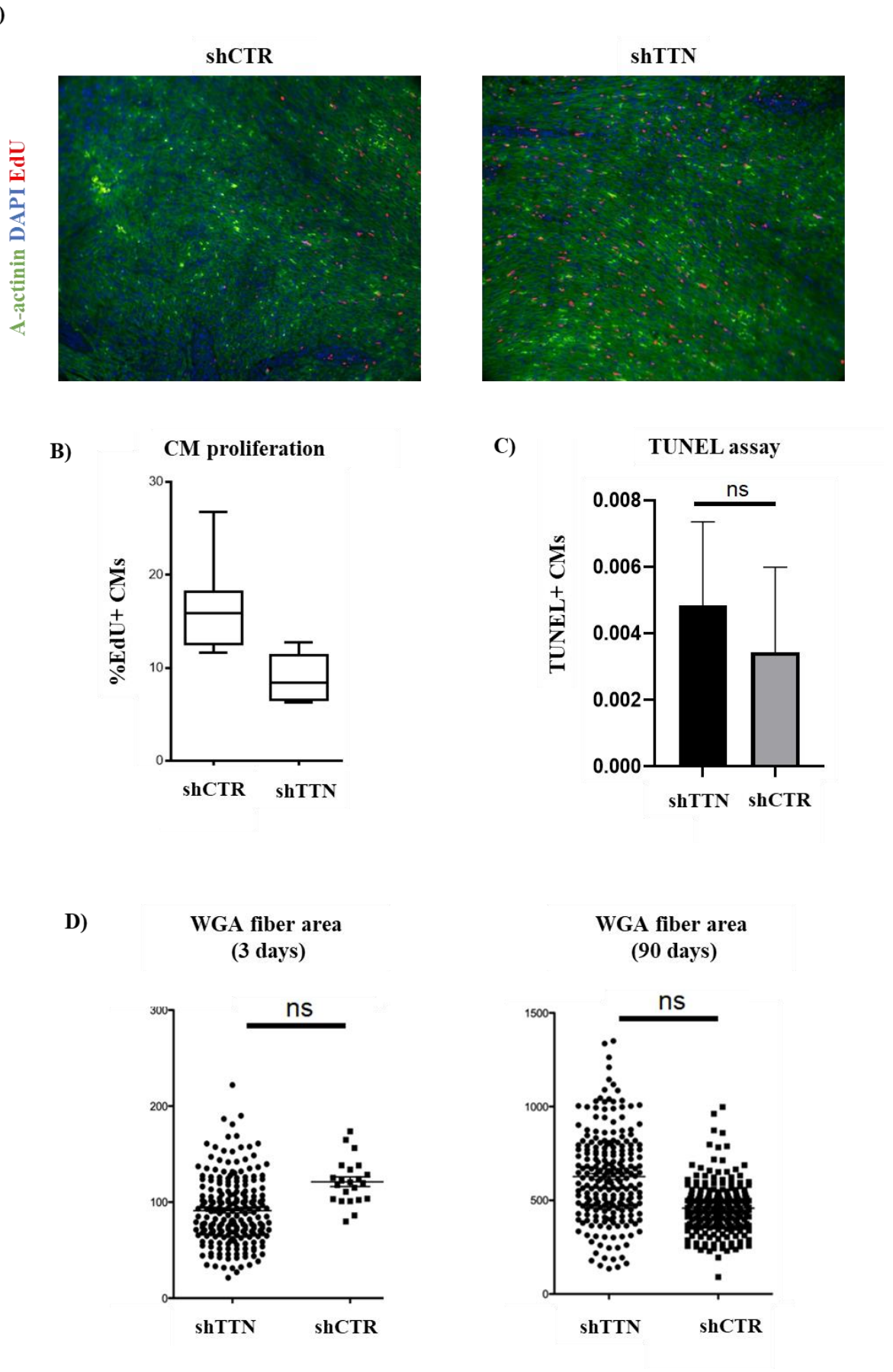
A)
shCTR
shTTN
A-actinin DAPI EdU
B)
CM proliferation
%EdU+ CMs
30
20
10
0
shCTR
shTTN
C)
TUNEL assay
TUNEL+ CMs
ns
0.008
0.006
0.004
0.002
0.000
shTTN
shCTR
D)
WGA fiber area
(3 days)
ns
300
200
100
0
shTTN
shCTR
WGA fiber area
(90 days)
ns
1500
1000
500
0
shTTN
shCTR

Figure 5

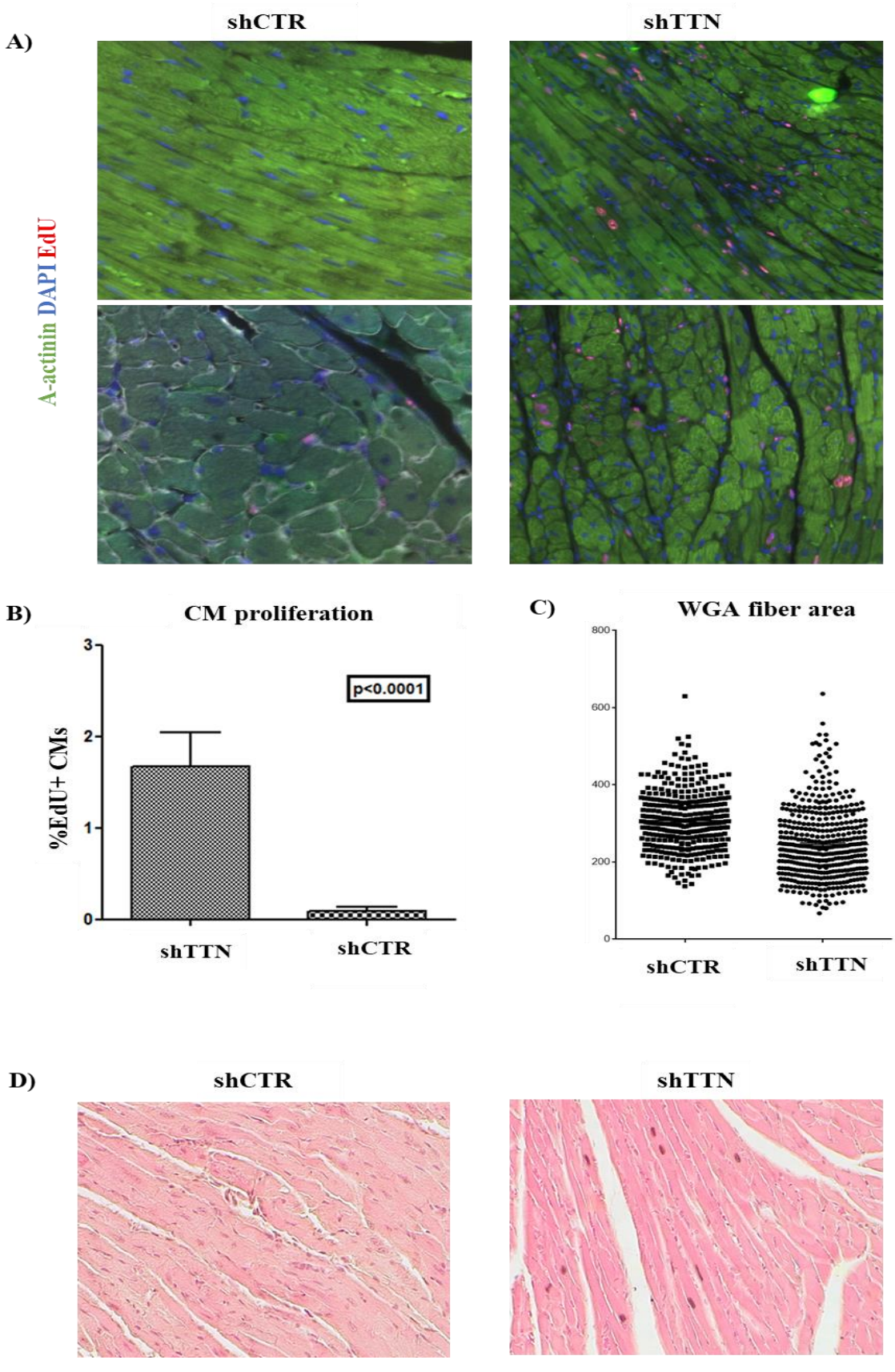
A)
shCTR
shTTN
A-actinin DAPI EdU
B)
CM proliferation
%EdU+ CMs
p<0.0001
shTTN
shCTR
C)
WGA fiber area
shCTR
shTTN
D)
shCTR
shTTN

Figure 6

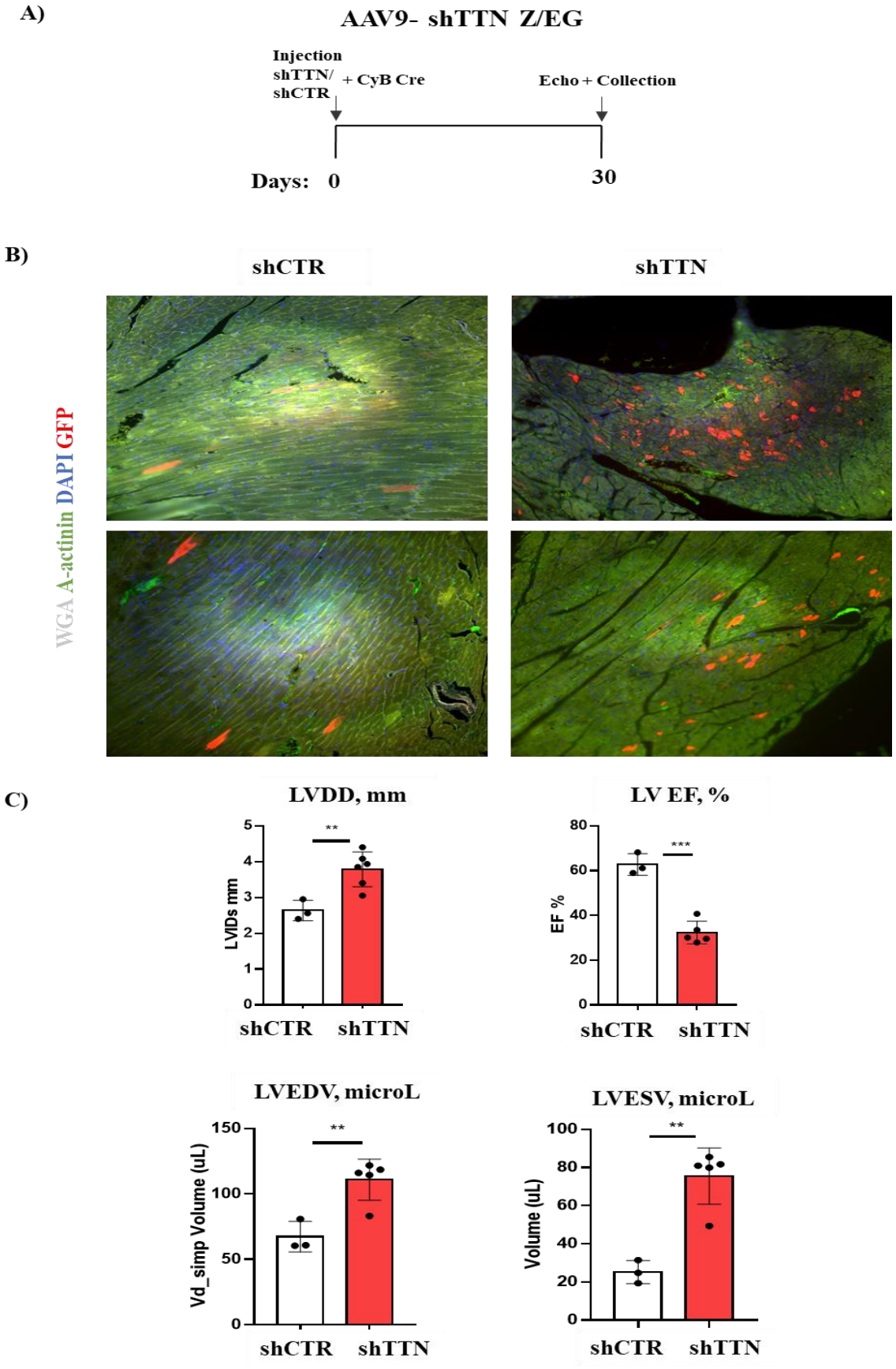
A)
AAV9- shTTN Z/EG
Injection
shTTN/
shCTR
+ CyB Cre
Echo + Collection
Days: 0
30
B)
shCTR
shTTN
WGA A-actinin DAPI GFP
C)
LVDD, mm
LVIDs mm
shCTR
shTTN
LV EF, %
EF %
shCTR
shTTN
LVEDV, microL
Vd_simp Volume (uL)
shCTR
shTTN
LVESV, microL
Volume (uL)
shCTR
shTTN

Figure 7

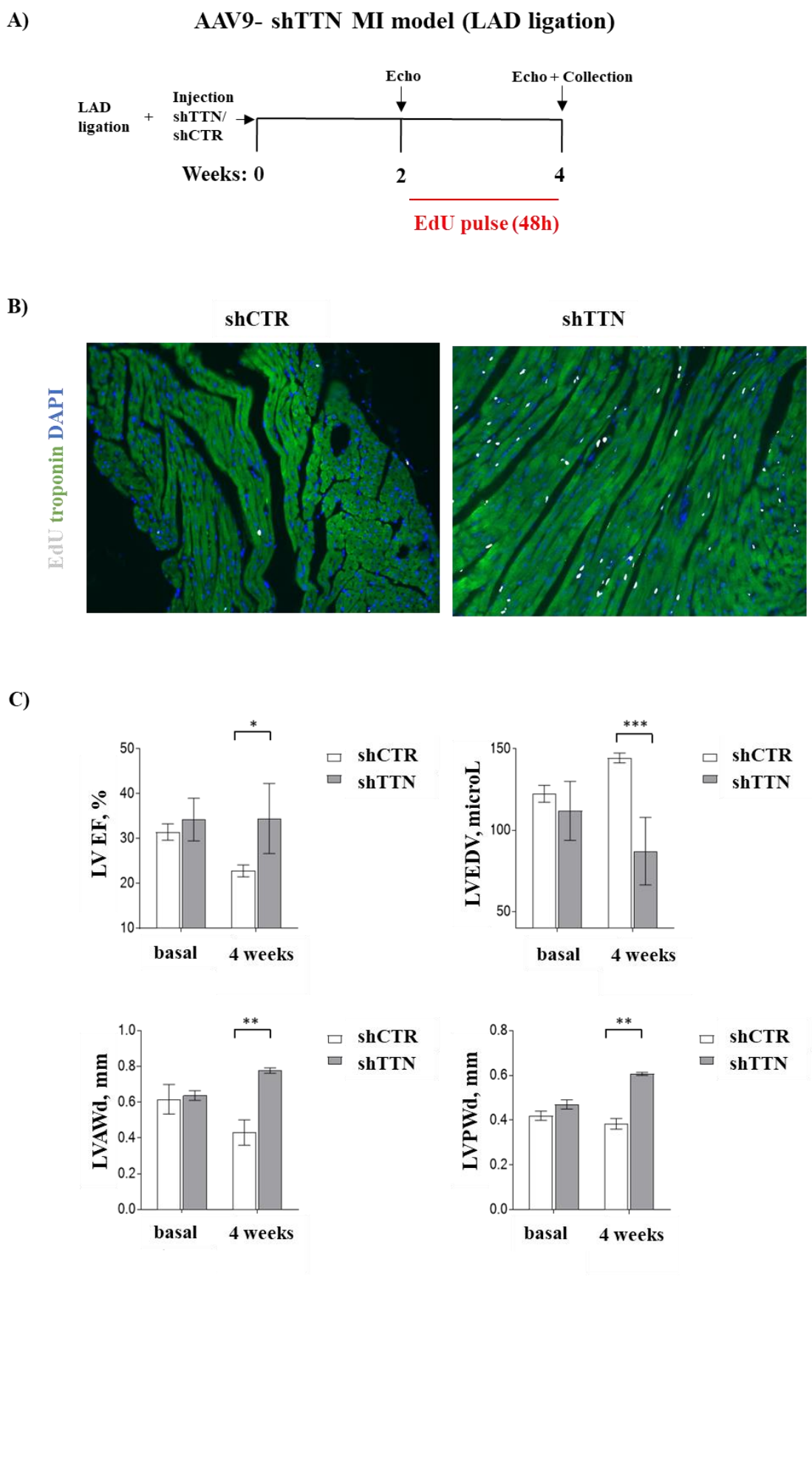
A)
AAV9- shTTN MI model (LAD ligation)
LAD ligation
+
Injection shTTN/ shCTR
Echo
Echo + Collection
Weeks: 0
2
4
EdU pulse (48h)
B)
shCTR
shTTN
EdU troponin DAPI
C)
LV EF, %
LVEDV, microL
LVAWd, mm
LVPWd, mm
basal
4 weeks
shCTR
shTTN
*
***
**

Figure 8

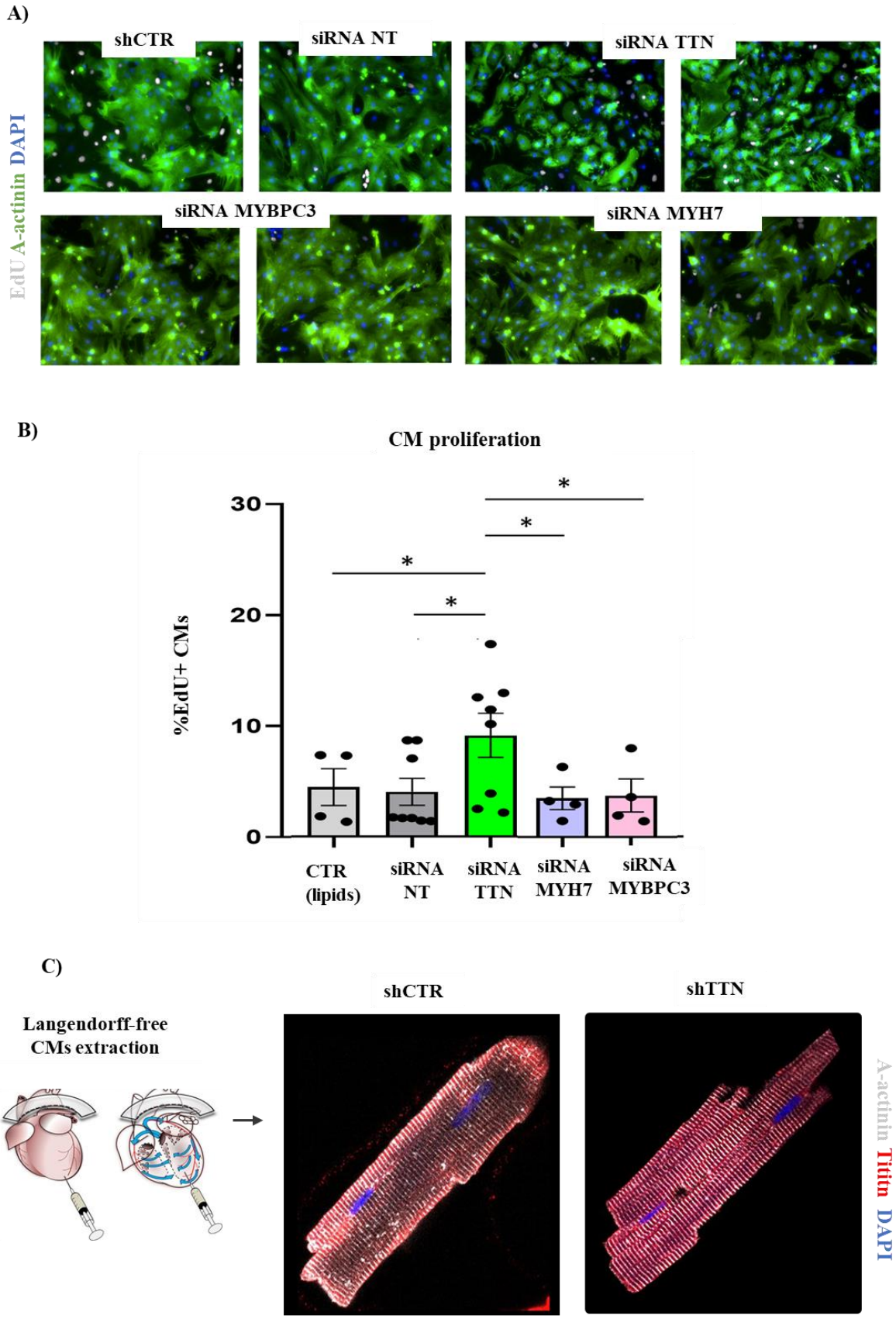
A)
shCTR
siRNA NT
siRNA TTN
siRNA MYBPC3
siRNA MYH7
EdU A-actinin DAPI
B)
CM proliferation
%EdU+ CMs
30
20
10
0
*
*
*
*
CTR (lipids)
siRNA NT
siRNA TTN
siRNA MYH7
siRNA MYBPC3
C)
Langendorff-free CMs extraction
shCTR
shTTN
A-actinin Titin DAPI

Figure 9

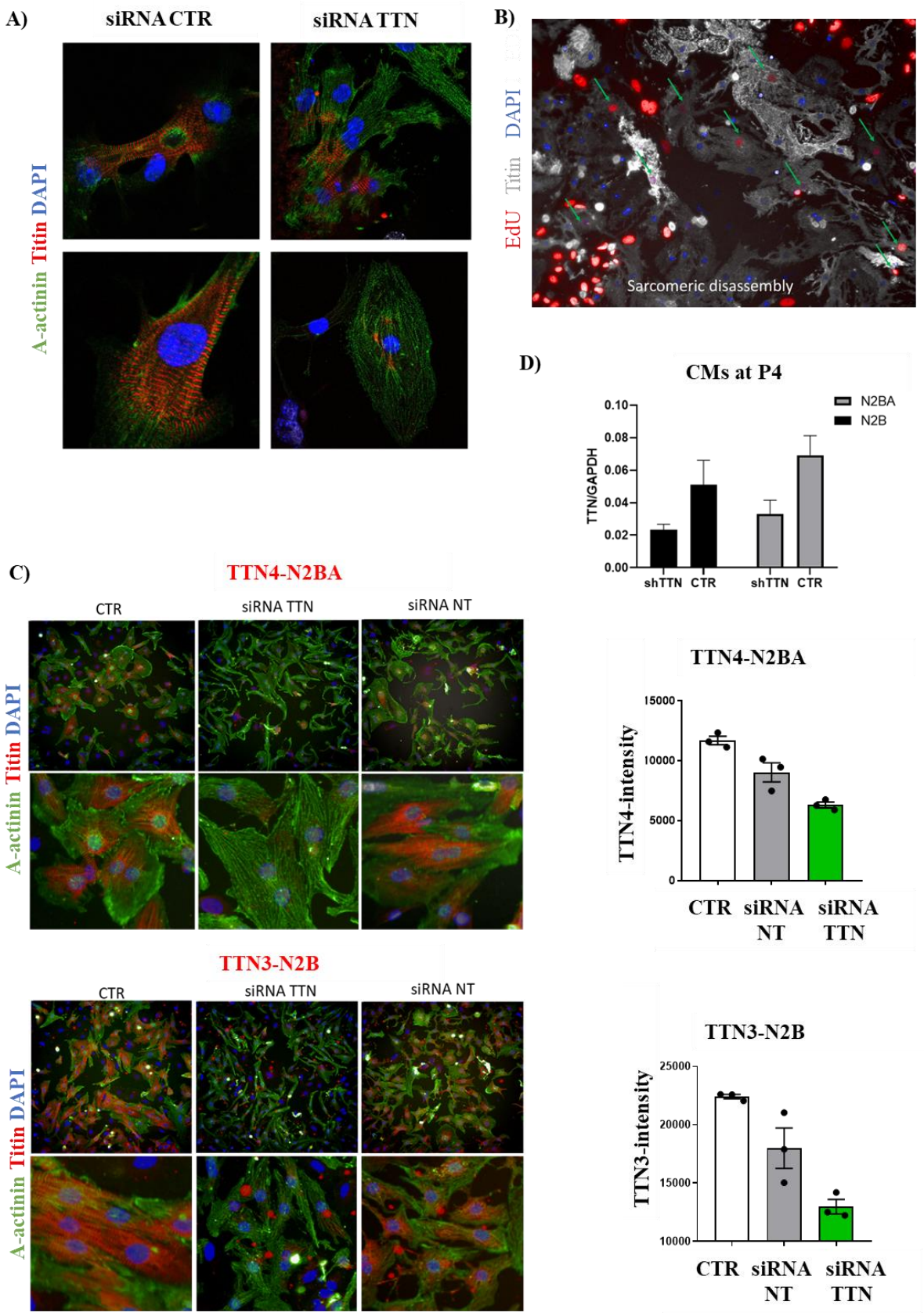
A)
siRNA CTR
siRNA TTN
A-actinin Titin DAPI
B)
EdU Titin DAPI
Sarcomeric disassembly
C)
TTN4-N2BA
CTR
siRNA TTN
siRNA NT
A-actinin Titin DAPI
TTN3-N2B
CTR
siRNA TTN
siRNA NT
A-actinin Titin DAPI
D)
CMs at P4
N2BA
N2B
TTN/GAPDH
0.10
0.08
0.06
0.04
0.02
0.00
shTTN CTR shTTN CTR
TTN4-N2BA
TTN4-intensity
15000
10000
5000
0
CTR siRNA NT siRNA TTN
TTN3-N2B
TTN3-intensity
25000
20000
15000
10000
CTR siRNA NT siRNA TTN

Figure 10

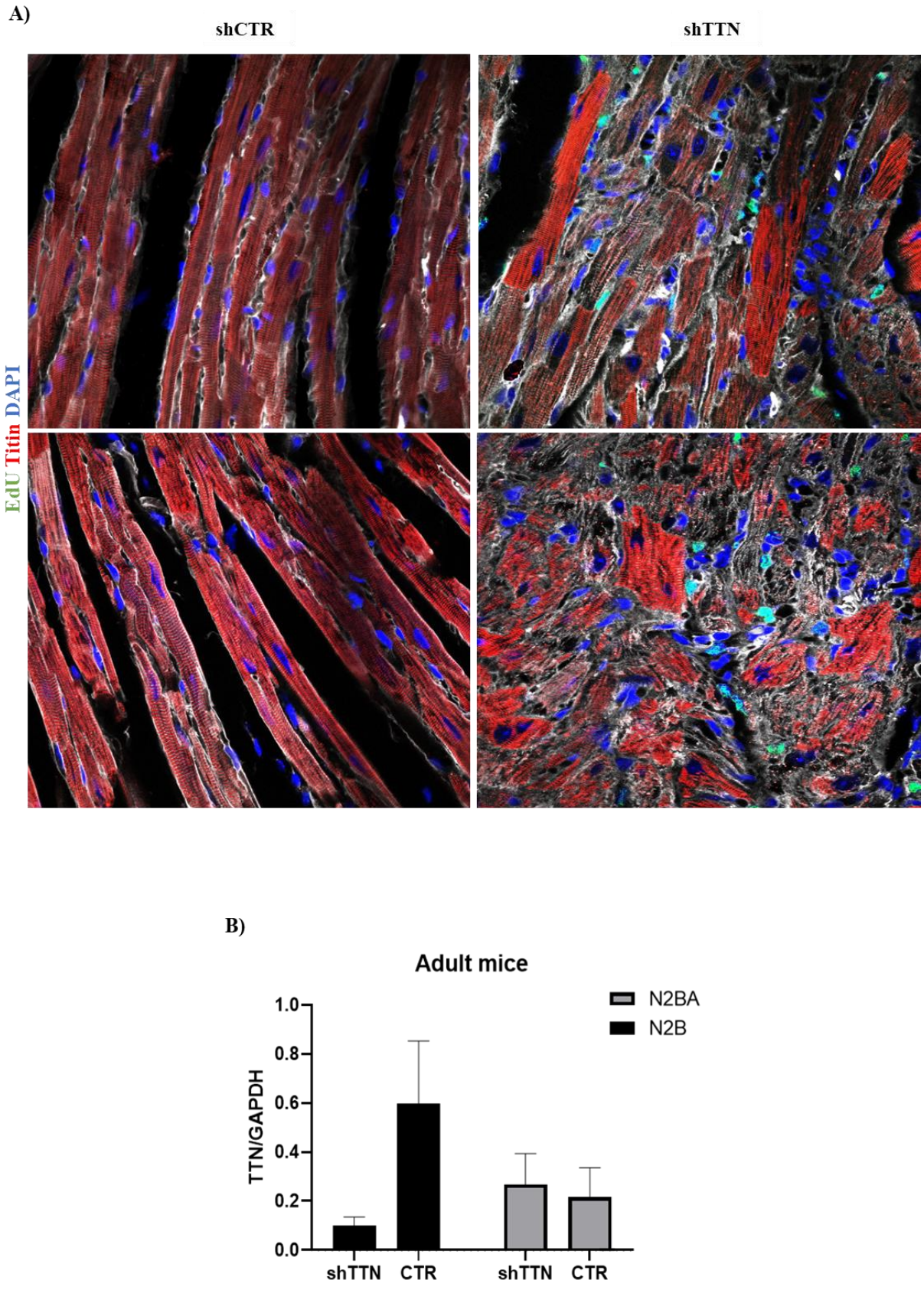
A)
shCTR
shTTN
EdU Titin DAPI
B)
Adult mice
N2BA
N2B
TTN/GAPDH
1.0
0.8
0.6
0.4
0.2
0.0
shTTN
CTR
shTTN
CTR

Figure 11

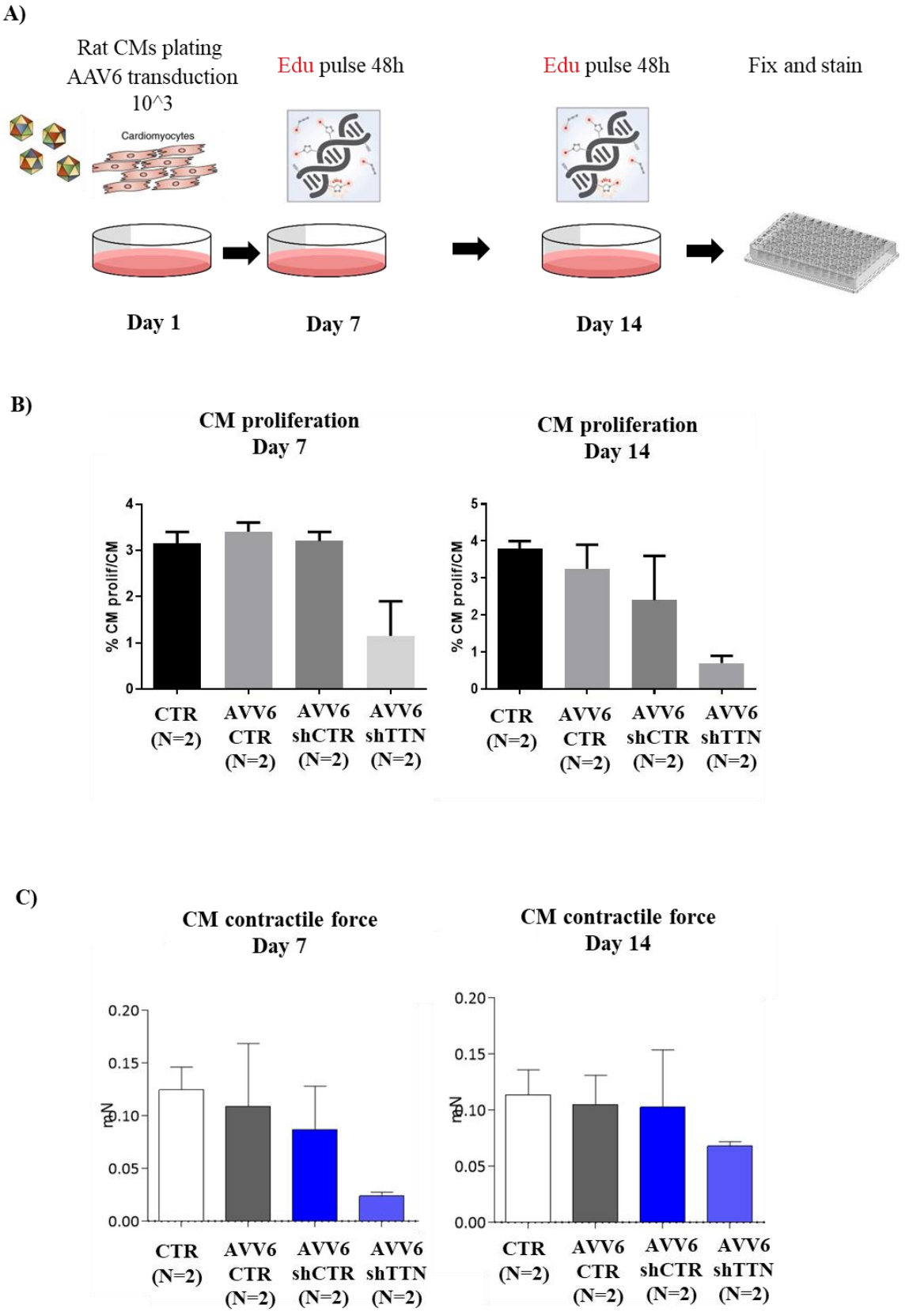
A)
Rat CMs plating
AAV6 transduction
10^3
Cardiomyocytes
Edu pulse 48h
Edu pulse 48h
Fix and stain
Day 1
Day 7
Day 14
B)
CM proliferation
Day 7
% CM prolif/CM
CTR (N=2)
AVV6 CTR (N=2)
AVV6 shCTR (N=2)
AVV6 shTTN (N=2)
CM proliferation
Day 14
% CM prolif/CM
CTR (N=2)
AVV6 CTR (N=2)
AVV6 shCTR (N=2)
AVV6 shTTN (N=2)
C)
CM contractile force
Day 7
mN
CTR (N=2)
AVV6 CTR (N=2)
AVV6 shCTR (N=2)
AVV6 shTTN (N=2)
CM contractile force
Day 14
mN
CTR (N=2)
AVV6 CTR (N=2)
AVV6 shCTR (N=2)
AVV6 shTTN (N=2)

Figure 12

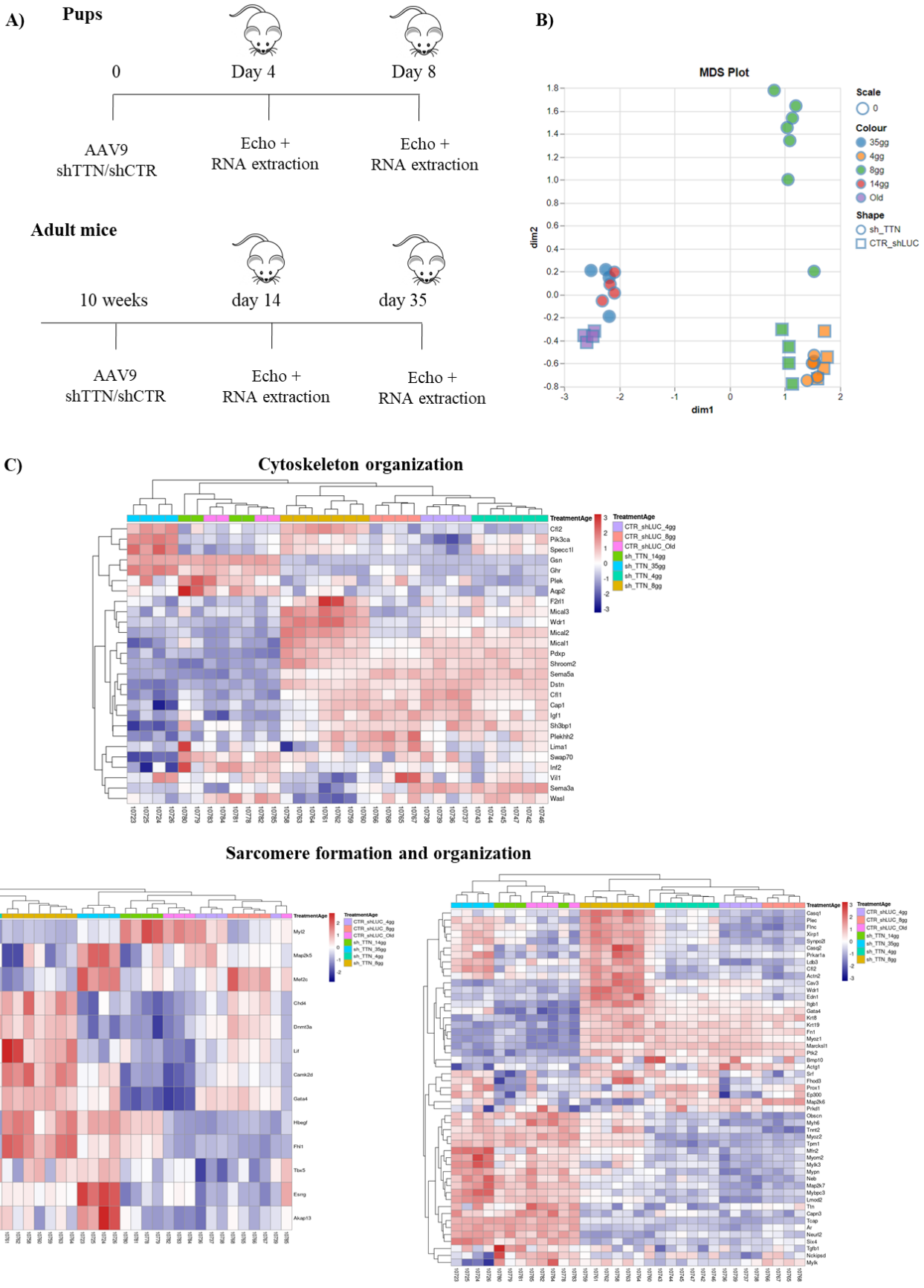
A)
Pups
0
Day 4
Day 8
AAV9
shTTN/shCTR
Echo +
RNA extraction
Echo +
RNA extraction
Adult mice
10 weeks
day 14
day 35
AAV9
shTTN/shCTR
Echo +
RNA extraction
Echo +
RNA extraction
B)
MDS Plot
dim1
dim2
Scale
0
Colour
35gg
4gg
8gg
14gg
Old
Shape
sh_TTN
CTR_shLUC
C)
Cytoskeleton organization
TreatmentAge
CTR_shLUC_4gg
CTR_shLUC_8gg
CTR_shLUC_Old
sh_TTN_14gg
sh_TTN_35gg
sh_TTN_4gg
sh_TTN_8gg
Cfl2
Pik3ca
Specc1l
Gsn
Ghr
Plek
Aqp2
F2rl1
Mical3
Wdr1
Mical2
Mical1
Pdxp
Shroom2
Sema5a
Dstn
Cfl1
Cap1
Igf1
Sh3bp1
Plekhh2
Lima1
Swap70
Inf2
Vil1
Sema3a
Wasl
Sarcomere formation and organization

Table 1

3 months	shTTN (5)	CRT (9)	p
Heart weight/ Tibia length	70,4±2,3	5,3±5,2	0,101
LVAWd, mm	0,61±0,04	0,68±0,16	0,456
LVDD, mm	4,17±0,24	3,91±0,06	0,180
LVPWd, mm	0,74±0,11	0,70±0,14	0,655
LVAWs, mm	0,81±0,11	1,12±0,27	0,053
LVDS, mm	3,52±0,29	2,64±0,09	**0,025**
LVPWs, mm	0,89±0,16	1,06±0,21	0,180
FS%	16,3±6,1	32,3±0,9	**0,025**
EF%	33,4±10,8	61,2±1,2	**0,024**
LV mass, mg	82,3±6,7	95,0±15,8	0,456
EF% (Simpson)	41,6±5,7	63,0±2,3	**0,025**
LVEDV, microL	89,3±16,7	60,5±7,6	**0,023**
LVESV, microL	52,7±15,0	22,4±3,3	**0,025**

EF, ejection fraction; FS, fractional shortening; LVAWd, left ventricular anterior wall thickness in diastole; LVAWs, left ventricular anterior wall thickness in systole; LAA, left atrial area; LVEDV, left ventricular end-diastolic volume; LVESV, left ventricular end-systolic volume; LVDD, left ventricle internal diameter in diastole; LVDS, left ventricle internal diameter in systole; LV mass, left ventricle mass; LVPWd, left ventricular posterior wall thickness in diastole; LVPWs, left ventricular posterior wall thickness in systole.

Table 2

5 weeks	shTTN (5)	CRT (8)	p
Heart weight/ Tibia length	79,3±2,3	64,1±5,2	**0,030**
LVAWd, mm	1,07±0,16	0,66±0,06	**0,003**
LVDD, mm	3,58±0,31	3,79±0,01	**0,008**
LVPWd, mm	1,04±0,12	0,74±0,06	**0,003**
LVAWs, mm	1,46±0,15	1,07±0,03	**0,003**
LVDS, mm	2,66±0,33	2,50±0,25	0,141
LVPWs, mm	1,37±0,10	1,07±0,03	**0,028**
FS%	25,9±3,4	34,0±6,3	0,223
EF%	51,8±5,7	63,3±8,9	0,291
LV mass, mg	149,4±23,7	91,3±10,7	**0,049**
EF% (Simpson)	51,7±7,8	55,0±4,3	0,143
LVEDV, microL	53,1±15,6	78,3±7,2	**0,019**
LVESV, microL	26,5±10,7	35,9±3,4	0,242
LAA, mm2	6±1,4	2,6±0,4	**0,018**

EF, ejection fraction; FS, fractional shortening; LVAWd, left ventricular anterior wall thickness in diastole; LVAWs, left ventricular anterior wall thickness in systole; LVEDV, left ventricular end-diastolic volume; LVESV, left ventricular end-systolic volume; LVDD, left ventricle internal diameter in diastole; LVDS, left ventricle internal diameter in systole; LV mass, left ventricle mass; LVPWd, left ventricular posterior wall thickness in diastole; LVPWs, left ventricular posterior wall thickness in systole.